Universidad de Investigación de Tecnología Experimental Yachay

Escuela de Ciencias Químicas e Ingeniería

TITULO: Study of the composition effect on the mechanical properties of a material made by Ecuadorian clay and sand for CO$_2$ capture.

Trabajo de integración curricular presentado como requisito para la obtención de título de Petroquímico

Autor:

Isaac Iglesias Palacios

Tutor:

Juan Pablo Tafur, PhD.

Co-tutor:

Edward Ávila, PhD.

Urcuquí, September 2020

SECRETARÍA GENERAL
(Vicerrectorado Académico/Cancillería)
ESCUELA DE CIENCIAS QUÍMICAS E INGENIERÍA
CARRERA DE PETROQUÍMICA
ACTA DE DEFENSA No. UITEY-CHE-2020-00056-AD

A los 12 días del mes de octubre de 2020, a las 16:00 horas, de manera virtual mediante videoconferencia, y ante el Tribunal Calificador, integrado por los docentes:

Presidente Tribunal de Defensa	Dr. VILORIA VERA, DARIO ALFREDO , Ph.D.
Miembro No Tutor	Dra. MORERA CORDOVA, VIVIAN , Ph.D.
Tutor	Dr. TAFUR GUISAO, JUAN PABLO , Ph.D.

El(la) señor(ita) estudiante **IGLESIAS PALACIOS, ISAAC ALEXANDER**, con cédula de identidad No. **1724979917**, de la **ESCUELA DE CIENCIAS QUÍMICAS E INGENIERÍA**, de la Carrera de **PETROQUÍMICA**, aprobada por el Consejo de Educación Superior (CES), mediante Resolución **RPC-SO-39-No.456-2014**, realiza a través de videoconferencia, la sustentación de su trabajo de titulación denominado: **STUDY OF THE COMPOSITION EFFECT ON THE MECHANICAL PROPERTIES OF A MATERIAL MADE BY ECUADORIAN CLAY AND SAND FOR CO2 CAPTURE**, previa a la obtención del título de **PETROQUÍMICO/A**.

El citado trabajo de titulación, fue debidamente aprobado por el(los) docente(s):

Tutor	Dr. TAFUR GUISAO, JUAN PABLO , Ph.D.
Co - Tutor	Dr. AVILA SOSA, EDWARD EBNER , Ph.D.

Y recibió las observaciones de los otros miembros del Tribunal Calificador, las mismas que han sido incorporadas por el(la) estudiante.

Previamente cumplidos los requisitos legales y reglamentarios, el trabajo de titulación fue sustentado por el(la) estudiante y examinado por los miembros del Tribunal Calificador. Escuchada la sustentación del trabajo de titulación a través de videoconferencia, que integró la exposición de el(la) estudiante sobre el contenido de la misma y las preguntas formuladas por los miembros del Tribunal, se califica la sustentación del trabajo de titulación con las siguientes calificaciones:

Tipo	Docente	Calificación
Miembro Tribunal De Defensa	Dra. MORERA CORDOVA, VIVIAN , Ph.D.	10,0
Tutor	Dr. TAFUR GUISAO, JUAN PABLO , Ph.D.	10,0
Presidente Tribunal De Defensa	Dr. VILORIA VERA, DARIO ALFREDO , Ph.D.	10,0

Lo que da un promedio de: **10 (Diez punto Cero)**, sobre 10 (diez), equivalente a: **APROBADO**

Para constancia de lo actuado, firman los miembros del Tribunal Calificador, el/la estudiante y el/la secretario ad-hoc.

Certifico que *en cumplimiento del Decreto Ejecutivo 1017 de 16 de marzo de 2020, la defensa de trabajo de titulación (o examen de grado modalidad teórico práctica) se realizó vía virtual, por lo que las firmas de los miembros del Tribunal de Defensa de Grado, constan en forma digital.*

IGLESIAS PALACIOS, ISAAC ALEXANDER
Estudiante

Dr. VILORIA VERA, DARIO ALFREDO , Ph.D.
Presidente Tribunal de Defensa

DARIO ALFREDO VILORIA VERA
Firmado digitalmente por DARIO ALFREDO VILORIA VERA
Fecha: 2020.10.12 17:40:11 -05'00'

Dr. TAFUR GUISAO, JUAN PABLO , Ph.D.
Tutor

Dra. MORERA CORDOVA, VIVIAN , Ph.D.
Miembro No Tutor

CIFUENTES TAFUR, EVELYN CAROLINA
Secretario Ad-hoc

AUTORÍA

Yo, **Isaac Alexander Iglesias Palacios**, con cédula de identidad 1724979917, declaro que las ideas, juicios, valoraciones, interpretaciones, consultas bibliográficas, definiciones y conceptualizaciones expuestas en el presente trabajo; así cómo, los procedimientos y herramientas utilizadas en la investigación, son de absoluta responsabilidad de el/la autora (a) del trabajo de integración curricular. Así mismo, me acojo a los reglamentos internos de la Universidad de Investigación de Tecnología Experimental Yachay.

Urcuquí, Septiembre del 2020.

Isaac Alexander Iglesias Palacios

CC: 1724979917

AUTORIZACIÓN DE PUBLICACIÓN

Yo, **Isaac Alexander Iglesias Palacios**, con cédula de identidad 1724979917, cedo a la Universidad de Tecnología Experimental Yachay, los derechos de publicación de la presente obra, sin que deba haber un reconocimiento económico por este concepto. Declaro además que el texto del presente trabajo de titulación no podrá ser cedido a ninguna empresa editorial para su publicación u otros fines, sin contar previamente con la autorización escrita de la Universidad.

Asimismo, autorizo a la Universidad que realice la digitalización y publicación de este trabajo de integración curricular en el repositorio virtual, de conformidad a lo dispuesto en el Art. 144 de la Ley Orgánica de Educación Superior.

Urcuquí, Septiembre del 2020.

_____

Isaac Alexander Iglesias Palacios
CC: 1724979917

ACKNOWLEDGMENTS

I want to thank God, family and friends who were throughout this stage of my university life.

I thank my family for all the support provided, specially my parents, brother and grandmother for all their love and values taught. Also, to my Friends who became my second family.

I thank the professors who helped me develop this work, specially my Advisors Juan Pablo Tafur PhD and Edward Ávila PhD for their time and advice given.

DEDICATION

To all my loved ones, for all the support and unconditional love.

Resumen

La captura y almacenamiento de carbono (CAC) ha sido una de las estrategias más estudiadas en la actualidad para mitigar las emisiones de CO_2, ya que es capaz de alcanzar el conjunto de objetivos propuesto en el acuerdo de París en el 2015 de almacenar al menos 1 Gt de CO_2 por año hasta el 2030. En la cadena del proceso de CAC, la captura y separación de CO_2 es el proceso más importante debido al gran costo energético que este representa. Entre las tecnologías de captura y separación de CO_2 disponibles, se encuentra el proceso de adsorción, en el cual se utilizan adsorbentes sólidos con el fin de separar el CO_2 de los otros gases efluentes. Actualmente, los adsorbentes que se han investigado son los MOFs, materiales mesoporosos de sílice, carbón activado, zeolitas, arcillas y óxidos metálicos. Muchos de estos adsorbentes sólidos durante el proceso de separación del CO_2 han demostrado problemas en la resistencia mecánica o capacidad de adsorción ante la humedad y temperatura elevadas. Por esta razón, en el presente trabajo se determinaron las propiedades mecánicas de un material alternativo en forma de pellas preparado a partir de arcillas y arenas ecuatorianas con alto contenido de óxidos metálicos para captura de CO_2. El material fue preparado a diferentes composiciones de arena ferruginosa utilizando la arcilla como aglomerante y soporte. Se sometieron a las muestras a la prueba de impacto de caída libre con el fin de obtener el número de caída en la cual se rompe y al ensayo de compresión uniaxial para determinar la resistencia a la compresión, el módulo de elástico y la tenacidad. Para la prueba de impacto de caída libre, se utilizaron muestras con porcentaje en peso de arena de 0 (muestra de control), 1, 5, 10, 15, 20, 25 y 50 % y se analizó la influencia del porcentaje de arena ante el impacto a la caída. Adicionalmente, se evaluó el comportamiento de pellas humedecidas a un porcentaje en peso de arena de 0, 15 y 25%. Con respecto al ensayo de compresión uniaxial, se sometieron a las muestras con contenido de arena en peso de 0, 15 y 25% a diferentes condiciones a la máquina universal de ensayos. Las condiciones utilizadas fueron muestras mezcladas con arena tamizada, arena sin tamizar y humedecidas. Para ambas pruebas se determinó el tipo de rotura ocurrido. Las fases minerales que componen las pellas fueron analizadas por difracción de rayos X y se cuantificó el contenido mineral mediante el método de refinamiento de ajuste del patrón completo de difracción en polvo.

Palabras clave: Propiedades mecánicas, pellas de arcilla y arena, adsorción de CO_2, prueba de impacto de caída libre, ensayo de compresión uniaxial.

Abstract

The Carbon Capture and Storage (CCS) has been one of the most strategies studied nowadays to mitigate the CO_2 emissions, since it is capable of achieving the set of objectives proposed in the Paris Agreement in 2015 of storing at least 1 Gt of CO_2 per year until 2030. In the CCS process chain, the CO_2 capture and separation is the most important process due to the high energy penalty which it represents. Among the available CO_2 capture and separation technologies, there is the adsorption process, in which solid adsorbents are used in order to separate the CO_2 from the other fluent gases. Currently, the adsorbents that have been investigated are MOF's, mesoporous silica, activated carbon, zeolite, clays and metallic oxides. Many of these solid sorbents during the CO_2 separation have shown problems in mechanical resistance or adsorption capacity against of humidity and high temperature. For this reason, in the present work, the mechanical properties of an alternative material in pellet form prepared from Ecuadorian clay and sands with high metallic oxide content for CO_2 capture were determined. The material was prepared with different ferruginous sand composition using clay as binder and support. The samples were subjected to the free-fall drop impact test in order to obtain the drop number in which they break and to the uniaxial compression test to determine the compressive strength, elastic module, and toughness. For the free-fall drop impact test, the samples with 0 (control sample), 1, 5, 10, 15, 20, 25 and 50 wt.% sand content were used and the influence of the sand percentage was analyzed against the impact to fall. Additionally, the behavior of the wet pellets was evaluated with a sand percentage of 0, 15, and 25 wt.% sand content. Regarding the uniaxial compression test, the samples with 0, 15, and 25 wt.% sand content were performed to the universal testing machine. The conditions used for samples were specimens with sieved sand, sand without sieved and under wet conditions. For both test, the type of fracture was determined. The mineral phases that make up the pellets were determined by X-ray diffraction and the mineral content was quantified using the whole powder pattern fitting.

Key words: Mechanical properties, clay/ sand pellets, CO_2 adsorption, free-fall drop impact test, uniaxial compression test.

CONTENT

LIST OF FIGURES

LIST OF TABLES

1. TITTLE

Study of the composition effect on the mechanical properties of a material made by Ecuadorian clay and sand for CO_2 capture.

2. INTRODUCTION-JUSTIFICATION

Power generation and certain industries such as refineries, cement plants and steel products are currently responsible for the high carbon dioxide (CO_2) emissions of into the atmosphere. Anthropogenic CO_2 is mainly the product of the burning of fossil fuels, which consequently has increased its concentration in the atmosphere. In 2019, the CO_2 concentration in the atmosphere was estimated to be approximately 410 ppm. CO_2 emissions in that year were around 37 Gt, an increase of 6% compared to the concentration in 2018[1]. The current CO_2 concentration in the atmosphere represents a significant increase compared to its concentration at the time of the industrial revolution (approximately 280 ppm)[2]. The increase in the CO_2 concentration has had negative effects, such as global warming and damage to the biodiversity. According to the Intergovernmental Panel on Climate Change (IPCC), if efficient mitigation measures are not taken, the CO_2 concentration in the atmosphere will increase to a range of 600 - 1550 ppm by 2030[3]. In the 21st session of the Conference of the Parties (COP) carried out in Paris in 2015 and rectified in the 25th session of COP performed in Madrid in 2019 have set as objectives that the temperature rise should be limited at a maximum of 1.5 °C and the global temperature increase should be kept down 2 °C compared to pre-industrial levels[4]. At present, the strategies that are in the development stage or are being applied for CO_2 mitigation are the efficient use of energy and energy conservation, the use of renewable energy (such as solar, wind, and hydroelectric energy as well as bioenergetics), the use of low carbon-intensive energy resources (such as hydrogen, nuclear energy and natural gas), the application of geoengineering initiatives (such as afforestation and reforestation), and the application of carbon capture and storage (CCS) technologies [5–7]. CCS denotes a set of technologies to reduce atmospheric CO_2 emissions generated by different human activities, especially energy production. It involves the use of technologies to capture and concentrate CO_2, transport it to a suitable storage place that does not affect the environment, and keep it isolated from the atmosphere for long periods[7]. Of all the stages involved in CCS technology, CO_2 capture has the higher energy

penalty associated with CO_2 separation, they represent about 70-80% of the total cost of the CCS chain process[8]. The capture techniques can be divided into two main groups: CCS technologies with CO_2 separation methods and CCS technologies that are not combined with CO_2 separation methods. The first group includes, pre-combustion and post-combustion while the second one comprises on oxy-fuel combustion and chemical looping combustion [9]. Regarding the first group, in precombustion, the CO_2 separation is produced before fuel burning. The main products that have to be separated are CO_2 and H_2. These gases are formed by gasification (coal) or steam reforming (fuel gas), followed by a gas shift reaction. On the other hand, in postcombustion the CO_2 separation occurs after fuel burning, resulting mainly in N_2, CO_2 and high parasitic load. An important disadvantage of postcombustion is the low CO_2 concentration (< 12 vol.% CO_2), low pressure (1-3 bar) and water content (3-10 vol.%)[10]. On the contrary, in precombustion there is more favorable separation conditions, the CO_2 concentration is higher, with a quantity of approximately 40% CO_2, and the effluent pressure is higher, with a value of approximately 35 bar[11]. Concerning the separation process, there are some technologies for isolating CO_2 over other flue gases, including chemical and physical absorption[12], adsorption[13], cryogenic-[14], membrane-[15], and hydrate[16]-based separation methods. Researches are increasingly developing and improving existing technologies in order to overcome the adversities that they present in the pilot phase or in the industries.

2.1 Adsorption

Adsorption process consists of removing CO_2 using a solid surface. The interaction between the mixed gas and the solid takes place on the adsorbent surface, therefore physical or chemical bonds are formed. The intermolecular forces are the driving force of this process. Some characteristics such as pore size, temperature, pressure and surface forces are important to the formation of a monolayer or multiple layers[9]. At industrial levels, adsorption towers are used to separate CO_2 from the other flue gases using a packing bed or fluidized bed in which the solid adsorbent interacts with the gas. The process begins by filling the tower with the solid adsorbent. After this, the gas passes through the packed bed, in which the gas which has more affinity with the adsorbent interacts and adheres to the solid surface until it gets saturated. Once saturated, the solid has to been regenerated by desorption to release the high concentrated CO_2 and reuse the solid for another adsorption cycles. Four technologies are available to the regeneration

cycle of the adsorbents such as pressure swing adsorption, temperature swing adsorption, electrical swing adsorption and vacuum swing adsorption[17]. Adsorption is considered among the other processes a potential candidate owing to its advantages over other separation methods, including the less-intensive energy consumption and economic regeneration process compared with other methods, simple operation and maintenance, satisfactory tolerance of moisture and impurities in the effluent, design flexibility for different applications and the low production of toxic wastes and corrosion[18].

2.2 Materials commonly used for adsorption

The solid sorbents used for CO_2 separation have been synthesized or pre-treated for achieving adequate porosity conditions for a better adsorption capacity[18]. Before the industrial use of these materials, certain requirements must be satisfied for optimal operational conditions, such as hydrothermal, chemical and mechanical stability, low cost of raw materials, regeneration capacity, selectivity, adsorption/desorption kinetics and low heat capacity[19]. The CO_2 adsorption performance is associated to the chemical surface and pore characteristics of the material. Also, the pressure conditions are related to the pore size in terms of CO_2 adsorption capacity. Concerning high pressure, the adsorption capacity is favored to porous materials which possess a higher surface area. In contrast, low pressure performs a better adsorption capacity for small surface area. There are 4 mechanisms for gas adsorption separation, for instance, molecular sieving effect, thermodynamic equilibrium effect, the kinetic effect, and quantum sieving effect[20]. Some typical porous materials for CO_2 adsorption process including MOFs, activated carbon, mesoporous silica, zeolites, and clay minerals. The selection criteria of the adsorbent depend on the best CO_2 adsorption capacity and selectivity. In fact, the nature of the adsorbent has to take into account, such as the size and the shape of the adsorbate molecule, the dipole moment, the quadrupole moment and the polarizability[21].

Table 1 summarizes some advantages and disadvantages of typical porous materials for CO_2 capture. Currently, researchers have studied some modifications to overcome the disadvantages of these materials. These modifications comprise in surface chemical treatment or functionalization of pore structure, cation exchange, amine impregnation, and nitrogen treatment[22–26].

Table 1: Summary of typical porous materials for CO_2 separation.

Porous material	Definition	Advantage	Disadvantage	Reference
MOFs	MOFs compounds are formed by metal ions and organic ligands, which contain N_2 and O_2. The porous structure could be one, two or three-dimensional. Volume, size, and chemical conditions of pore depending on the design of it. This could be modified or changing by organic ligands, altering the concentration on the reactants, the temperature reaction and reaction times, pH of the solution, the ratio of metal/ligand.	-Large CO_2 adsorption capacity -Potential selectivity for CO_2 - Handling pore structure and pore surface properties	-Relatively low thermal and chemical stability due to weak coordination bonds -Undesirable perturbations on chemical or structural properties. -Costly production at industrial scale	[6, 27–30]
Activated carbon	Activated carbon can be considered as any carbonaceous material which contains high carbon content. In order to enhance the pore properties, a physical or chemical activation treatment is needed. The physical activation consists of applying high temperature, followed by oxidation, to leads the enhancement of pore characteristics. Chemical activation consists of undergoing the material with a dehydrating agent, for instance, bases, acids, or salts at about 600 °C and 800 °C.	-Low water affinity -High adsorption capacity -Low cost -Low energy requirement for regeneration -High stability -Safe for local environment -High resistivity to alkaline and acidic conditions	-CO_2/N_2 low selectivity -Hardly controllable structure in terms of pore size. -Non-uniformity structure -Weak CO_2 binding -Various precursors for activation.	[31–34]
Mesoporous silica	Mesoporous silica are materials synthesized from soluble silica and self-organized aggregates of surfactants, which produce a pore size between 2 and 50 nm. MCM-14, MCM-48, HMS and SBA-15 are the most prominent silica materials which stand out since large surface area, narrow pore size distribution and the ability to control the pore. A remarkable property of this silica material is the feasibility of surface modification to prepare materials with desirable properties and applications	-Controllable structure in terms of pore size. -Ordered structure -Fast adsorption kinetics	-Most porous silica shows relatively low hydrothermal stability. -Presence of water usually decreases the adsorption capacity.	[35–37]
Zeolites	Zeolites are porous crystal aluminosilicates mineral, either natural or synthetic, which have a high surface area and molecular sieving properties. Zeolites contain a three-dimensional framework formed by cavities and channels in which small molecules, ions and entities may penetrate reside which are the basis of their molecular adsorption.	-Quicker adsorption of CO_2 -Lower energy penalty in the process -Low cost -Safe for local environment -CO_2/N_2 high selectivity -Well developed structural chemistry	-Adsorption capacity reduced over time due to water vapor -Reduces of adsorption capacity al low temperature and wet conditions.	[26, 31, 38–40]
Clay minerals	In a broader sense, clay minerals refer to any mineral which size is shorter than two micrometers. The soils and rocks weathering process involves physical disaggregation and chemical decomposition that change the original minerals from silicates to clay minerals.	-Low cost and abundant availability -Potential to synthesize other adsorbents improving the CO_2 adsorption capacity -High mechanical and thermal stability.	-Clays requires an extra treatment to achieve adsorption capacity. -Relatively low CO_2 adsorption compared to other porous material. -Poor textural properties	[41, 42]

Additionally to the mentioned porous materials, exist other materials which are used for CO_2 adsorption based on chemical adsorption. The mechanism of these materials depending on the adsorbate, in general it leads to the carbonates and bicarbonates formation. Metal oxides have been used as an adsorbent, the typical alkali earth metal is CaO, many studies determine that it has good properties for adsorption; however, the regeneration step requires high energy demand (approximately 900 °C). Researches have proposed alternative metal oxides to CO_2 adsorption, for instance, titanium oxide nickel oxide, silver oxide, lanthanum sesquioxide, cerium oxide, copper oxides, and iron oxides[43].

2.3 Clay and ferruginous sand in Ecuador

Ecuador is located in South America, with a surface area of 283.560 Km^2. This country has 24 Provinces, which are divided into four regions, including the coast, highlands, amazon, and the insular region, resulting in a variety of geological scenarios. Consequently, there are favorable geological conditions that allow the mineral formation, for instance, metallic minerals, non-metallic minerals, and clay minerals[44]. Concerning clay and non-metallic minerals, the exploitation of this sector is designated to manufacture a variety of materials, either artisanal manufacturing or industrial production. Depending on the mineral clay content and the process, the result product could be ceramic, glass, cement refractories, and pieces of calcined clay. A study made by Rafael Uribe[45] showed the distribution of some occurrences of raw materials. It is important to remarkable the difference between minerals occurrences and mineral reservoirs. On the one hand, minerals occurrences refer to a geological area of interest but not in the economic interest, while mineral reserves evaluate the technological, economical, and feasible to extract.

According to Uribe[45], 44% of mineral clay occurrences are in the exploitation stage, while 54% are in the exploration phase. Regarding non-metallic mines, 47% of occurrences are dedicated to artisanal manufacture of bricks and tiles to meet the demand in each province in which it is developed, 14% is dedicated to the industrial sector to produce fine ceramic, and the 39% remaining is in analyzing step to determine the feasibility of an industrial ceramic application. Before the manufacture of materials is important to taking into account the clay properties, such as adsorption and absorption capacity, swelling, ion exchange, and plasticity[46].

Figure 1 describes the non-metallic occurrences percentage per Ecuador Province. They are divided into feldspars, kaolin, clay, and rest of non-metallic occurrences. Feldspars comprise of clays formed mainly by feldspars mineral group while kaolin is constituted principally of kaolinite. Clay refers to common primary clays with a variety of minerals. Finally, the rest of the non-metallic occurrences include sand, limestone, mica, graphite, and others which in this case is not of interest[45]. Additionally, Figure 1 does not include Santa Elena, Santo Domingo, Galapagos and Orellana.
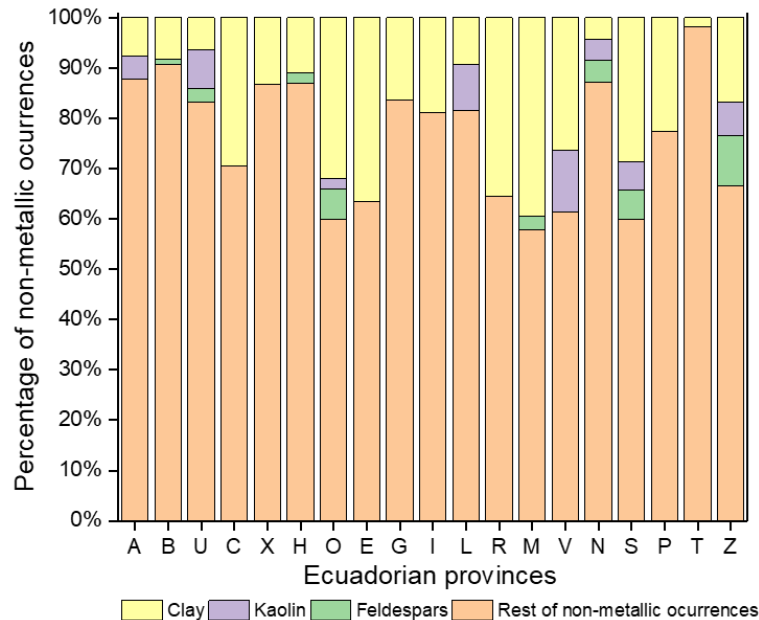
Figure 1: Percentages of non-metallic mineral occurrences in Ecuadorian provinces. The Provinces' nomenclature are the following: Azuay (A), Bolivar (B), Cañar (U), Carchi (C), Cotopaxi (X), Chimborazo (h), El Oro (O), Esmeraldas (E), Guayas (G), Imbabura (I), Loja (L), Los Rios (R), Manabí (M), Morona Santiago (V), Napo (N), Pastaza (S), Pichincha (P), Tungurahua (T), Zamora (Z) [45].

Concerning ferruginous sands, they are natural mixtures of iron oxides with metal traces such as aluminum, titanium, and copper. The main ferruginous sand mining in Ecuador is carried out in Esmeralda province, in the canton Muisne. The sand reservoir is denominated Playa Negra, also known as Suspiro's Beach. The exploitation area is known as Ostional Bloque 1, which comprises a surface area of 22 hectares. Currently, the cement industry is the main sector that uses the ferruginous sand, with the purpose of increasing the iron percentage in the Portland cement to enhance the material resistance. Other secondary ferruginous sand deposits are located in Manabí and Guayas Provinces which are also used for fabricating Portland cement. In contrast, the deposit located in Santa Elena Province is used to glass opaque, as a refractory or chemical product due to the titanium dioxide separation from magnetite and other impurities[47].

2.4 Mechanical properties of a material[48]

Characterizing a material by mechanical testing is an important step previous its use to simulate the service conditions to which the material will be subjected. The tensile, compression, flexure, and shear tests are assays in which a static load is applied over a cross-section or surface. Concerning to compression, the load applied to the sample is performed in a universal testing machine (UTM). The main goal of this test is to determine the material resistance and the deformation against an applied compressive force. The compression test is preferentially applied to fragile materials, for instance, concrete, ceramic, and materials made of clay. In contrast, the tensile essay is carried out for ductile materials such as steels, metals, and plastics. The testing material must be manufactured following the norms dictated by American Society for Testing and Materials (ASTM). The results thrown by the UTM, in general, are in terms of force (kN) vs. deformation (mm) curve, this result depends on the specimen size. For this reason, it is necessary to normalize to avoid this sample size dependent. When the parameters are normalized, the result that they show are Stress versus Strain curve. To get the Stress parameter is necessary to divide the force (F) by the initial area (A_o) of the sample (Ec. 1)

$$\theta = \frac{F}{A_o} \qquad \qquad \text{(Ec. 1)}$$

The units of stress is MPa, resulting in the relation of force in kN and area in mm^2.

On the other hand, the Stain (ε) is defined as:

$$\varepsilon = \frac{\Delta L}{L} = \frac{L_o - L_i}{L_o} \qquad \qquad \text{(Ec. 2)}$$

Where L_o represents the initial length before the compression and L_i denotes the instantaneous length.

To analyze the behavior of the material through the compression is necessary to graphic the curve strain in function of the stress.

Figure 2 shows two sections, the elastic region (blue color) and the elastic region (pink color). The elastic region refers to the non-permanent deformation of the material, it means that the initial length will be kept when removing the load at any point within this region. Regarding the plastic region, when the load is removed, the deformation is

permanent, therefore, the material will not recover its original shape. Besides, there are five points: A, B, C, D, and E.
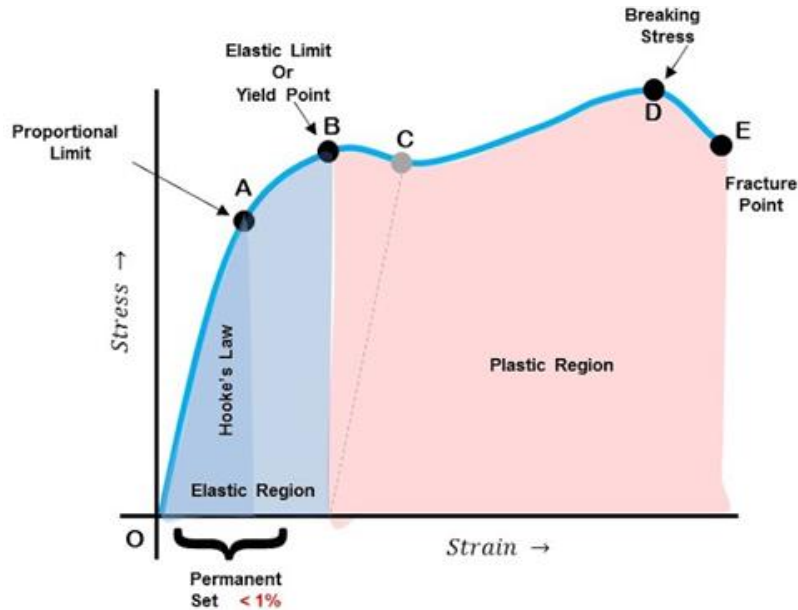
Figure 2: Stress versus Strain diagram[49].

- Point A: The proportional limit indicates the final point of the lineal behavior; above these values the stress is not proportional to the strain.
- Point B: The yield point is the transition between the elastic region and the plastic region.
- Point C: Lower yield stress point.
- Point D: The breaking stress is the maximum stress that a material can stand before it fractures. It is also known as compression strength for compressive test. In general, it cannot be perceived by sight.
- Point E: The fracture point refers to the visibility of the fracture in the specimen.

From the stress vs. strains curve, some mechanical properties can be calculated, for instance, the elastic module, the compressive strength, and toughness.

The elastic module is a parameter that characterizes the elastic behavior of a material. From a molecular perspective, it can be seen as a measure of the atoms resistance separation, that is, the interatomic bonding forces. If the elastic module shows a linear

behavior in all the elastic zone, it follows the Hooke law and is known as the Young modulus. The elastic module can be defined as the relation of stress and strain:

$$E = \frac{\theta}{\varepsilon} \qquad \text{(Ec. 3)}$$

Where E is the elastic modulus (E), ε represents the stress (MPa), and θ denotes the strain (mm/mm).

To process a large amount of data, the Ec. 3 has to modify in order to obtain the equation of the line, of the form:

$$y = a\mathrm{x} + \mathrm{b} \qquad \text{(Ec. 4)}$$

For this, it is necessary to clear from the equation the stress, by the following way:

$$\theta = E * \varepsilon \qquad \text{(Ec. 5)}$$

In this way, the Ec. 4 and Ec. 5 have the same form, so it can be estimated the elastic modulus by linear regression, where θ represents y, ε denotes x, and E refers *a* from the equation of the line.

In some materials, the elastic behavior is not linear and cannot be calculated by the Young Module, for this reason is necessary to use an alternative method, for instance, tangent or secant modulus. The tangent modulus is taken as the slope of the stress-strain curve at some specified level of stress, while secant modulus represents the slope of a secant drawn from the origin to some given point (Figure 3).
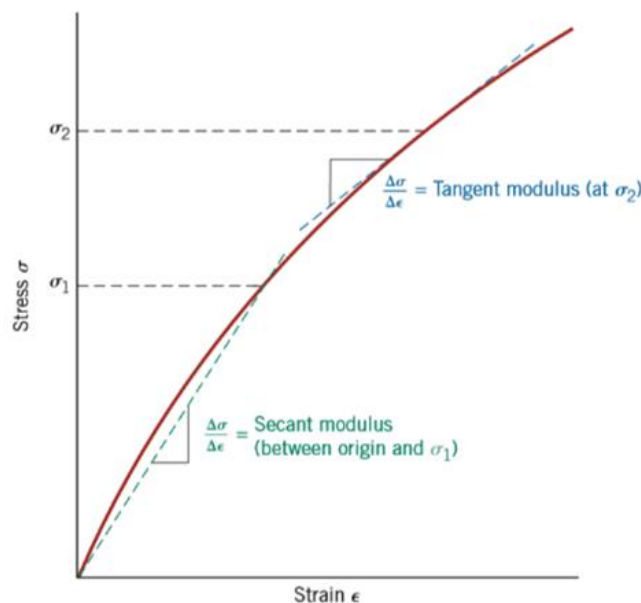
Figure 3: Non-linear behavior of some materials in the elastic region[48].

The compressive strength represents the maximum load that a material can support under compressive forces. From the force vs. elongation curve, this data can be estimated by dividing the crushing force by the cross-sectional area (Ec. 6). In contrast, from the stress vs. strains diagram, the compressive strength can obtain directly estimated the maximum peak.

$$Rs = \frac{C_f}{A} \qquad (Ec. 6)$$

Where Rs is the compressive strength (MPa), C_f represents the crushing force (kN) and A the cross-sectional area (mm^2).

The mechanical properties associated with energy is the resilience and toughness (Figure 4). Resilience is the capacity of a material to absorb energy without any plastic deformation. To quantify the resilience, it is necessary to integrate the elastic region of stress vs. strain curve with the following equation:

$$Ur = \int_0^{\varepsilon_y} \theta \, . \, d\varepsilon \qquad (Ec. 7)$$

Where Ur represents the resilience (J/m^3 or Pa), ε_y is the strain at yielding (mm/mm), and θ refers to stress (MPa).

Finally, the toughness is the total energy absorbed from material before its fracture due to stress or impact. The toughness could be estimated by integrating the area under the stress vs. strain curve. The equation which describes this behavior is:

$$T = \int_0^{\varepsilon_r} \theta \, . \, d\varepsilon \qquad (Ec. 8)$$

Where T is the toughness (J/m3 or Pa), ε_r represents the strain at rupture point (mm/mm), and θ denotes the stress (MPa).

Figure 4: Resilience (green area) and toughness (yellow area) of stress vs. strain curve[48].

Several factors lead to uncertainties in measuring data, in consequence, the data may have scattered for mechanical properties. This could be associated with factors such as the test method, variation in sample preparation procedure, operator bias, inhomogeneous wit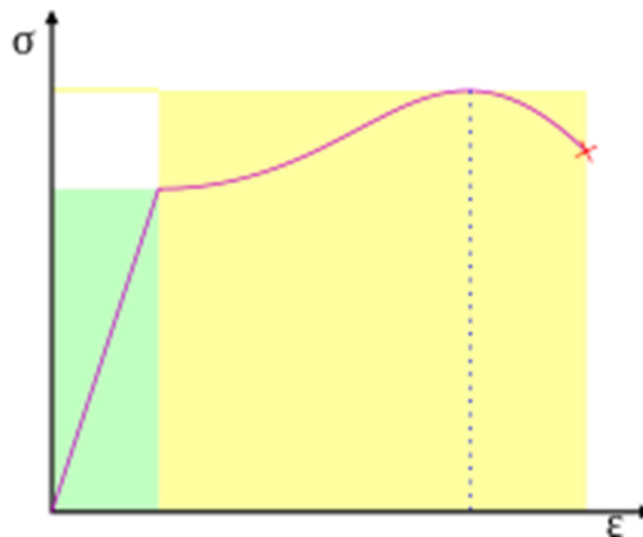hin the same material lot, slightly different composition of materials in the same lot, and apparatus calibration. Therefore, it is necessary to apply a statistical method to estimate the dispersion degree. For this, the average and the standard deviation should be calculated. The average value is calculated by dividing the sum of all measured values by the number of measurements taken. The equation that describes the average is the following:

$$\bar{x} = \frac{\sum_{i=1}^{n} X_i}{n} \qquad \text{(Ec. 9)}$$

Where $\bar{x}$ is the average, X_i is the value of a discrete measurement and n is the total samples number.

Concerning standard deviation, it represents the error or degree dispersion of the data. The expression which describes the standard deviation is the following:

$$S = \left[\frac{\sum_{i=1}^{n} X_i - \overline{X^2}}{n-1}\right]^{1/2} \qquad \text{(Ec. 10)}$$

Where $\bar{x}$ is the average, X_i is the value of a discrete measurement and n is the total samples number.

3. PROBLEM STATEMENT

The increase of CO_2 concentration into the atmosphere since the industrial revolution is approximately 45%, mainly caused by anthropogenic CO_2. Several strategies are available to mitigate the CO_2 emissions, however the Intergovernmental Panel on Climate Change (IPCC) concluded that these strategies do not meet the requirements to mitigate the high amounts of CO_2 produced into atmosphere. In fact, the cost of these strategies represents a higher value of about 138% of the average of all the strategies, except for CCS[50]. The CCS process represents a potential strategy for achieving the COP objective. Among the CCS chain process, the CO_2 capture and separation are the most important due to the high energy penalty of the process. Among all the existing technologies, adsorption demonstrates important advantages over the other technologies. In the adsorption process, porous materials commonly are used in the form of packed bed into adsorption towers and have to accomplish some criteria for their use, one of them is the mechanical

resistance during the operational conditions with the purpose of scaling up. For scaling up these type of materials is important the study of mechanical properties due to commonly suffer abrasion or crushing owing to the operational conditions causing by volumetric flow rate, vibration, and temperature. The sorbents have to demonstrate microstructure and morphological stability during the CO_2 adsorption and regeneration steps[28]. For this reason is important to determine the mechanical properties of a material previous their industrial use due to the breakage of the adsorbents leads to problems in the process, causing economic and environmental consequences.

4. GENERAL AND SPECIFICS OBJECTIVES

4.1 General objective

To determine the mechanical properties of an innovative material based on a mixture of natural clay and ferruginous sand in pellets form for CO_2 capture.

4.2 Specific objectives

- To perform the pellets to the free-fall drop impact test in order to determine the drop number of the samples.
- To evaluate the mechanical resistance of the samples by uniaxial compression test with the purpose of determining the compressive strength, the elastic module and the toughness.
- To characterize by X-ray diffraction the material with the aim of identify the mineral composition of the samples.

5. METHODOLOGY

5.1 Raw materials and initial treatment

The clay samples used were taken from Yantzaza, located in Zamora Chinchipe Province, Ecuador. These samples were dried in an oven at 100 °C for 12 h as the initial treatment[51]. Ferruginous sands were taken from Ancon, located in Santa Elena Province, Ecuador. The sand samples were previously dried at 100 °C for 8 h[52], and then a portion of the samples was sieved. For the sieving process, 7 stainless steel sieves from Retsch in Germany were used, and the sieves numbers were ½, 1, 4, 8, 16, 30 and 50. Finally, the grain size obtained was 300 μm[51].

5.2 Sample preparation for mechanical testing

The pellet preparation was performed manually. First, clay was weighed and mixed with different amounts of sieved sand (to promote their homogeneous dispersion in the mixtures), with the purpose of obtaining samples with sand content of 0 (control sample), 1, 5, 10, 15, 20, 25 and 50 wt.%. Then, distilled water was added with a dropper (approximately 8% of the total volume), and a 13 mm (diameter) spherical mold (Figure 5) was used to shape the pellets. Finally, the samples were calcined in a Boeco muffle furnace with a temperature ramp of 5°C/ min until reaching 450 °C over 14 h.

Figure 5: Spherical mold used for shaping the pellets[53].

The cylindrical specimens were done similar to pellets, the differences are stated on the 13x26 mm cylindrical mold used (Figure 6a and 6b) and the sand conditions. In these samples, clay was mixed with different quantities of sieved sand and sand that had not been sieved to obtain specimens 0, 15, and 25 wt.% sand content. To analyze the wet conditions, all the samples were left to rest in distilled water for 6 days. The selected

quantities of 15 and 25 wt. % of sand content is based on the commercial chemical Sulfatreat-410 HP, in which the iron oxide concentration is in a range of 10-30 wt.%[54].
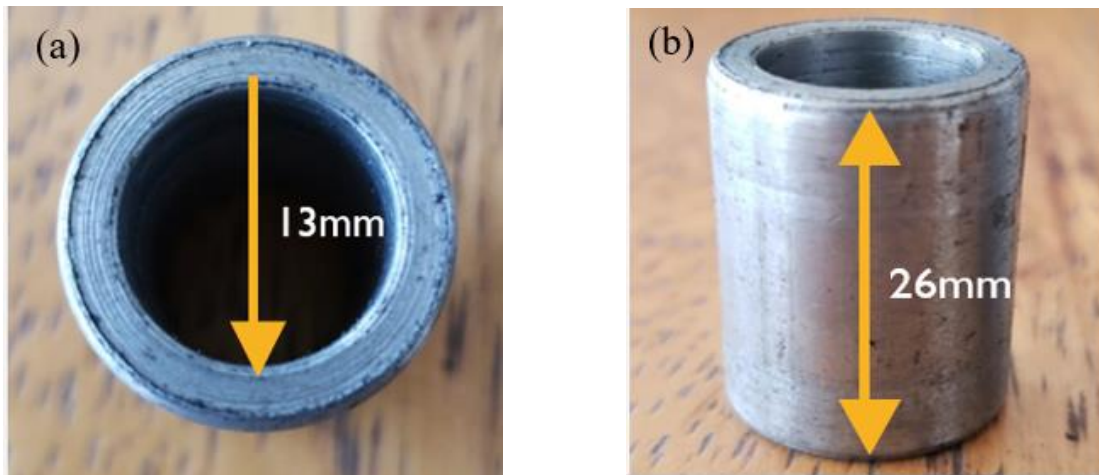
Figure 6*: Cylindrical mold used for shaping the specimens: (a) top perspective showing the diameter measurement, (b) front perspective showing the length measurement[53].

The prepared samples were labeled based on the clays and sands nomenclature worked a in previous work[51]. The samples were divided into three different groups:

- The first group was attributed to the samples mixed with sand that was not sieved denominated CZY-304 / SYA-104 R X%. In order to facilitate the nomenclature, the sample was named C304-104 R X%

- The second group refers to samples mixed with sieved sand denominated CZY-304 / SYA-104 S X%. In order to facilitate the nomenclature, the sample was labeled C304-104 S X%.

- The last group denotes for samples in wet conditions denominated CZY-304 / SYA-104 S X%. In order to facilitate the nomenclature, the sample was called C304-104 W X%.

For all the samples, X% represents the sand content by weight expressed in a percentage.

5.3 Mechanical property determination

Before the mechanical properties determination, it is important to measure the relative porosity and determine the height and diameter of the samples. The relative porosity percentage was estimated once the pellets were prepared and calcined to contain 0, 15, and 25 wt.% sand. First, three samples were weighed 3 times with an analytical balance. Then, they were allowed to rest in distilled water for 6 days. Finally, samples were

removed from distilled water and weighed again on an analytical balance. The Ec. 11 was used for calculating the relative porosity percentage.

$$\% \text{ Porosity} = \frac{m_f - m_i}{m_f} * 100 \qquad \text{(Ec. 11)}$$

Where m_f is the mass after 6 days of resting in water and m_i is the initial mass.

To measure the height and the diameter of the samples a gauge ruler was used. Concerning the diameter, the specimens were measured at the top, in the middle, and at the bottom. To estimate the height of the specimens there was measured from 3 different perspectives. Finally, for both measurements, the average was calculated.

5.3.1 Free-fall drop impact test

The free-fall drop impact test and the uniaxial compression test were used to determine the mechanical properties of the pellets. The free-fall drop impact test was performed by dropping the pellets from a height of 1.5 m on a tile surface (Figure 7). With the help of a Nikon camera, the falls were filmed to obtain the number of rebounds and the height of each rebound. At least 7 tests were performed for each pellet, and each trial had a minimum of 7 repetitions or until the pellet broke. At the moment in which the pellet showed a rupture, the drop number was reported.

Figure 7: Free-fall drop impact test.

From the free-fall drop impact test, the coefficient of restitution (COR) can be estimated. The COR describes the energy conservation degree in a collision between classical particles. In the case of a collision between a particle and a fixed body, the case is

considered as one dimension rebound. The equation which describes this behavior is the following:

$$COR = \sqrt{\frac{h_o}{h_f}} \qquad \text{(Ec. 12)}$$

Where h_o is the initial height (1.5 m) and h_f is the height reached in the rebound. Values nearly to 0 express an inelastic collision, while values near to 1 state an elastic collision. The coefficient of restitution is dimensionless.

5.3.2   Uniaxial compression test

The uniaxial compression test was performed with a United DSTM electro-mechanical series universal testing machine (UTM). The compression was performed at a constant velocity of 10.9 µm/s. This test follows the ASTM D2166 standard. At least 7 specimens were tested with the UTM. The information provided by the UTM gave the diagram force versus elongation relationship, hence it was normalized using Ec. 1 and Ec. 2.

Several data were estimated by the uniaxial compression test using the equations describes previously, for instance the compressive strength (Ec. 6), the elastic module by linear regression (Ec. 5), toughness (Ec. 8), and the crushing strength (maximum peak from the force vs deformation diagram). Additionally, in order to analyze the data dispersions degree, the main (Ec. 9) and the standard deviation (Ec.10) were calculated.

5.4 Sample characterization powder by X-ray diffraction

The crystalline phase identification is very important in solid materials characterization owing to the mineral composition influences on the mechanical, physical and chemical properties. To carry out this characterization the samples were ground up in an agate mortar to a fine powder. After that, each sample was mounted in an aluminum sample holder on a multipurpose stage with 8-positions. The X-ray diffraction (XRD) analysis was carried out by a powder diffractometer Mini-flex-600, from Rigaku, with D/tex ultra 2 detectors. The measurement conditions were 40 kV and 15 mA for the X-ray generator in a sealed tube with a $CuK_{\alpha1,2}$ radiation source. For collecting data, the selected angular region was $2\theta = 5\text{-}90°$ with a step width of $0.005°$. The data treatment was carried out using Qualx 2.8[55] and SmartLab Studio 4.3 programs. In both cases, the crystallography open data (COD) base was used as the powder diffraction database[56]. The data reduction (the smoothing, background and zero-point corrections, and peak search) of powders diffraction was possible in each program. In this case, it was necessary to employ the

search-match methodology[57] to obtain the list of the possible candidates as a constituent of the crystalline phases present in clay, sand and mixtures. With the purpose of quantifying the crystalline phases of the samples, the whole powder pattern fitting methodology (WPPF) was applied[58]. This method allows us to find more appropriately the relative abundance percentage of the crystalline phases present in samples. The samples analyzed were pellets with sand content of 0, 15, and 25 wt.%. Also, sieved ferruginous sand (SYA-104) was analyzed, but in this case, it was carried out in two different ways. The first method used the sieved sand content in its natural state, and the other method used magnetically separated sand. For the magnetically separated sand, the metallic oxides that possessed magnetic properties were isolated with a magnet (2 Tesla) from the sand. Therefore, two different samples were obtained, one that was separated by the magnet labeled enriched metallic ferruginous sand (E.M. ferruginous sand) and the remaining part labeled non-magnetic ferruginous sand (N.M. ferruginous sand).

6. RESULTS, INTERPRETATION AND DISCUSSION

6.1 Mechanical properties

The evaluation of the mechanical properties of the prepared pellets is necessary for its industrial scale-up for CO_2 capture purposes. An adequate mechanical resistance is required to evaluate the filling behavior of the pellets in an adsorption tower and stability of the packed bed during the operation to avoid breakage of pellets. Besides, if the pellets production plant is far from the plant of interest, the transport process implies the necessity of a good mechanical resistance. The pellet quality was assessed as a function of the sand content quantity in the pellets by free-fall drop impact test. In contrast, the uniaxial compression test was used to analyze the influence of mineral composition, porosity, and humidity by compressive forces in the samples.

6.1.1 Free-fall drop impact test

The free-fall drop impact test is intended to provide information about the response of pellets to a collisions that occurs during handling, for instance, adsorption tower filling activities. Concerning to dry samples, the behavior of the drop number in function of sand content in pellets is shown in Figure 8.
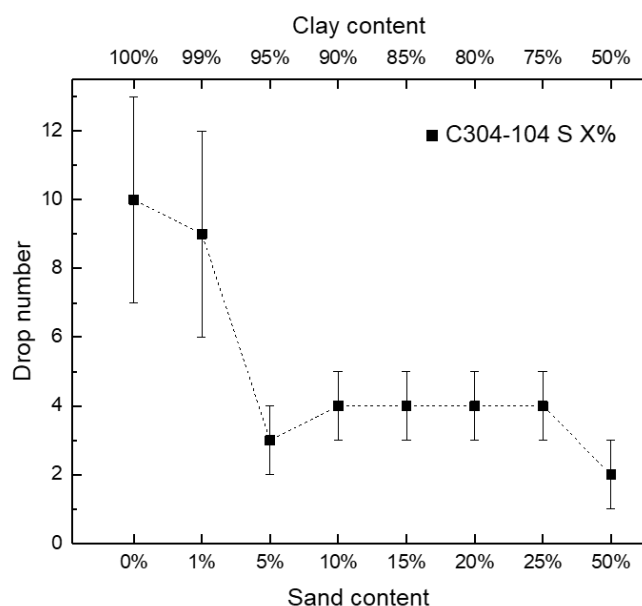

Figure 8: Drop number in function of sand content for dry samples.

Regarding the control sample (C304), it exhibited an average of 10 drops. The sand content in pellets affected the drop number significantly, due to it was added sand to the samples, the drop number decreases. It was evidenced since C304-104 S 1% the drop

number decreases one unit compared to C304. The drop number suffered a drastic drop from C304-104 S 1% (9 drops) to C304-104 S 5% (3 drops) and remained almost constant with a drop number of 4 until C304-104 S 25%. This suggests that the sand content in pellets for the free-fall drop impact test does not have a linear behavior, this means that the sand addition to the samples is not proportional to the drop number.

Regarding the wet samples, pellets with sand content of 0, 15 and 25 wt.% were performed to the free-fall drop impact test. The drop number showed the same behavior compared to samples at dry conditions, for instance the control sample (C304) and C304-104 S 25% (overlapped in Figure 9). The difference marked the pellets C304-104 S 15%, which at wet conditions exhibited a slight increment in their drop number with 5 drops compared with the same sample in dry condition. The results suggests that the wetting samples does not affect the drop number of the pellets.
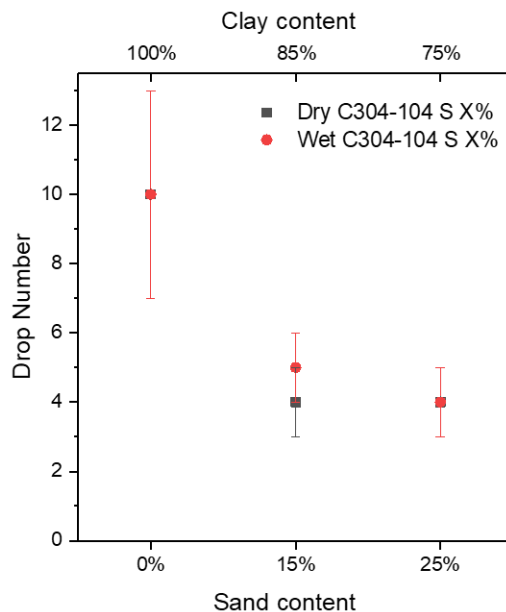
Figure 9: Comparison of the drop number for dry and wet samples at 0, 15 and 25 wt.% sand content

According to Tavares & de Almeida[59], the drop number for meeting the handling requirement of dry pellets should be at least 4, therefore all the samples in this study can be considered suitable for handling, except the samples C304-104 S 5% and C304-104 S 50%, which barely resisted 3 and 2 drops respectively. Some factors influence the pellets behavior, causing variations in their physical and mechanical properties such as the drop number. Gul et al.[60] mentioned some of these factors, for instance, the type of clays used as a binder, moisture, surface area, pellet size, and pelletizing condition. In this case, the grains uniformity is not the same owing to the particle size difference between clay and sand. Thus, it can be deduced that the particle size uniformity due to the increase of sand

content influences the mechanical resistance of the pellets against free-fall drop impact test.

After the free-fall drop test, it was analyzed the type of breakage which pellets experimented. The pellet fracture showed two behaviors, a superficial rupture and a pellet body breakage (Figure 10). The superficial or surface rupture refers to a break in which the pellets remain intact and small cracks occur causing a slight mass loss in the form of finer chips, this type of rupture is also called attrition, abrasion, wear, or chipping. In contrast, the body breakage comprises a loss of the original pellet integrity, in which a representative mass loss is evidenced in different particles size[61].
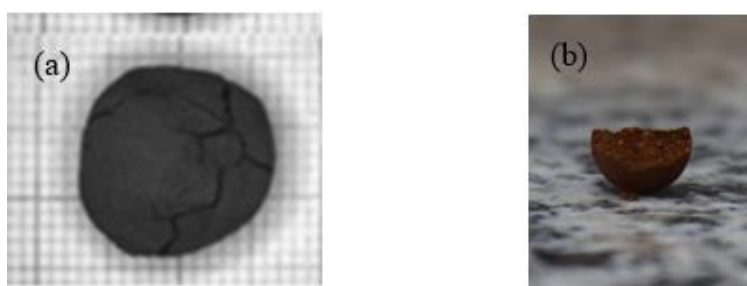

Figure 10: Pellets breakage after free-fall drop impact test: (a) surface breakage with low mass loss[62], (b) body breakage with approximately 50% mass loss.

Tavares & King[63] stated that the probability of pellets breakage is proportional to the repeated impact and the stress in which the pellets are subjected. At lower impact energy or stress, the surface breakage probability is dominant over a pellet body breakage, also the pellets strength decrease for each impact. On the contrary, at moderate impact energy or stress, the pellets suffer a transition from surface breakage to body breakage. Finally, at higher impact energy or stress, the pellets have a higher probability of body breakage. In this work, it was evidenced that although the height (1.50 m) for the free-fall drop impact test was the same for all samples, the pellets have experimented surface and body breakage, this suggests that the sand content in pellets affected the breakage mechanism. It was evidenced that the dry control samples showed a surface rupture and even withstood at least one extra fall before a body breakage (for most of control samples). This behavior was evidenced also for the sample C304-104 S 1%. On the contrary, for the most of the samples with 5, 10, 15, 20, and 25 wt.% sand content demonstrated a surface rupture, but in this case the pellets suffered a body breakage after an extra fall. The sample C304-104 S 50% showed a body breakage, which means lower pellet resistance. Concerning the wet samples, the rupture mechanism was surface breakage for all the pellets. The wet control samples showed a surface rupture, in contrast to the dry

control sample they did not resist an extra fall after a surface rupture. The wet samples C304-104 S 15% and C304-104 S 25% showed the same behavior compared to the dry samples.

It is important the study of the type of pellets breakage and the mechanical impact resistance, due to it involves economic and environmental implications. The fines and particle size generation due to the pellets body breakage may lead to an extra removing treatment, owing to these particles could fill the void spaces among the pellets that make up the packed bed, causing a reduce of the porosity into the adsorption tower, therefore the gas flow could be disturbed and also causing a drop pressure. Concerning environmental implication, the fines represent a problem owing to the dust generation during pellets transportation[64]. According to Sivrikaya & Arol[65] the dust generation from pellets is related with the surface roughness. The authors argue that pellets with smooth surface and low strength generate lower dust compared with the pellets with high strength and rough surfaces. The mechanism of the dust generation is based on the attrition and impact forces during the pellets handling. In this case, the breakage mechanism of pellets which contained 1, 5, 10, 15, 20, and 25 wt.% sand content favors the filling process of the adsorption tower. This is because in the case of a rupture, the pellets will not experiment a mass loss, therefore it would not affect the packed bed porosity.

Commonly in the free-fall drop impact test, the pellet does not break in the first drop due to the particle orientation during the impact and the absence of defects causing by a previous impact[66]. Instead of this, the particle impacted the surface and conserved a part of the energy in the form of rebound. The degree of energy conservation can be related to the coefficient of restitution estimated with Ec. 12 (Table 2 and Table 3). On the other hand, the part of energy which does not transform into rebound leads to the formation of microfractures into pellets. As the pellets experimented more impacts, the microfractures propagate at the point of a rupture of the samples[67].

Table 2: Coefficient of restitution values for dry samples performed to the free-fall drop impact test on a tile surface.

Sample code	Coefficient of restitution ± 0.0305
C304	0.4680
C304-104 S 5%	0.3380
C304-104 S 10%	0.4286
C304-104 S 15%	0.4193
C304-104 S 20%	0.3695
C304-104 S 25%	0.4083
C304-104 S 50%	0.1507

Table 3: Coefficient of restitution values for wet samples performed to the free-fall drop impact test on a tile surface.

Sample code	Coefficient of restitution ± 0.0256
C304 W	0.3910
C304-104 W 15%	0.3523
C304-104 W 25%	0.3086

Table 2 shows the coefficient of restitution of dry samples performed to the free-fall drop impact test. The results are values around in the range of 0.3300 to 0.4700 for all samples, except for C304-104 S 50% which showed lower values of about 0.1507. These results express inelastic collision behavior, especially the sample C304-104 S 50%, this means that most of the energy was transformed in fracture propagation than in rebound, which lead to a quicker rupture[61]. This can be related to the lower values of the drop number. Also, the sample C304-104 S 5% showed a slight low value compared to the other samples, however in this case the samples could have fallen in the same orientation, making the pellets rupture more easily. The samples C304-104 1% cannot be reported because technical issues, however it was expected that the results should be similar than the control samples.

Table 3 indicates the coefficient of restitution of wet samples that contained 0, 15 and 25 wt.% sand. The results showed lower values compared to dry samples at the same sand content, which means that moisture in the samples could affect the rebound; however the drop number was the same in both conditions.

6.1.2 Uniaxial compression test

The uniaxial compression test gives important data to estimate some mechanical properties such as the elastic module, the compression strength, and the toughness of the samples. The compressive strength could provide an idea of the pellets behavior which make up the packed bed under the operational conditions in adsorption towers and also

in pellets transportation. The mineral composition, humidity, and porosity play important roles in the behavior of the samples under compression forces, in fact this could be evidenced in the 3 different conditions of specimens. The results showed different tendencies of the specimens with regard to the mechanical properties. It is important to clarify that certain samples showed failures during compression, so they were not taken into account.

The relative porosity percentage of pellets decreases as the amount of sand increases for samples of 0, 15 and 25 wt.% sand content (Table 4). This could be related to the sand content which filling the void spaces.

Table 4: Relative porosity percentage of pellets performed to uniaxial compression test.

	C304	C304-104 S 15%	C304-104 S 25%
Relative porosity (%)	17.99	16.83	14.54

The highest values of compressive strength were for the samples C304-104 S 15%, followed by C304-104 R 15% (Figure 11). Concerning the control sample (C304), it has demonstrated lesser compressive strength compared to samples with sand content (Figure 11a and 11b). There was expected that the control sample showed higher compressive strength because the non-presence of sand; nevertheless, samples with 15 wt.% sand content demonstrated higher values. This could be related to the relative porosity, due to the compressive strength is inversely proportional to the porosity. According to Howarth & Rowlands[68] the high porosity is the reason why micro-facture networks are created and the tension distribution through the samples under the effect of compressive forces. Although the samples C304-104 S 25% showed the lesser porosity percentage, the compressive strength values were not higher. This could be attributed to the mineral composition, because under compressive forces, minerals with higher hardness such as hematite, quartz and ilmenite showed breakage at lower stress due to the contact with other soft mineral phases. The control sample at wet condition, C304-104 W 15%, and C304-104 W 25 % demonstrated the least compressive resistance compared to their same concentrations in dry conditions. Different behaviors were observed under wet conditions than under dry conditions, for instance the compressive strength values decrease as the quantity of sand increases as showed Figure 11.
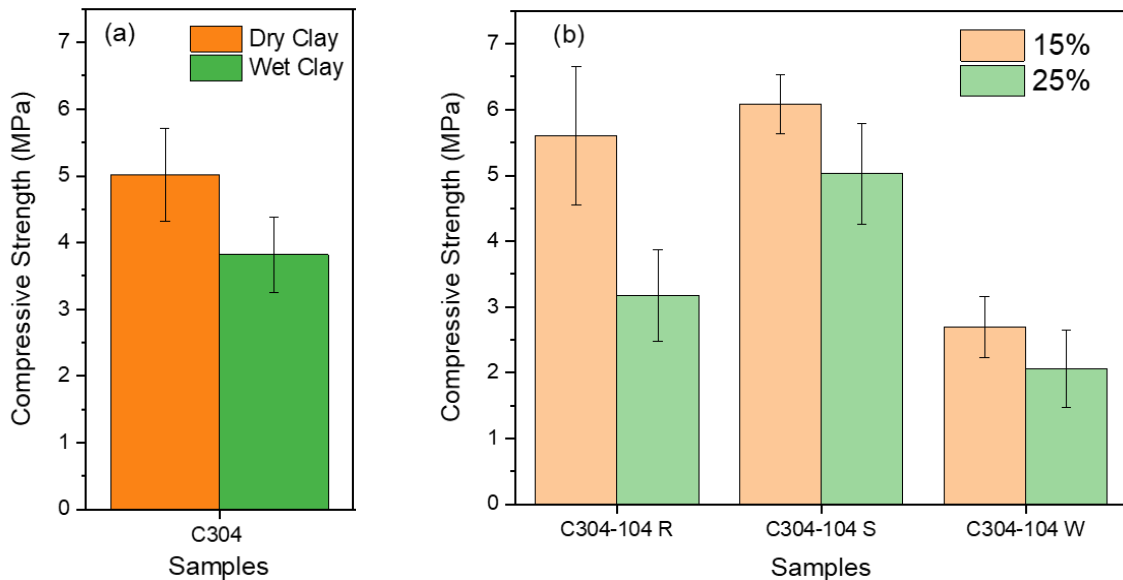
Figure 11: Compressive strength for specimens: (a) dry and wet control sample specimens, (b) specimens with sand content at the 3 different conditions: sand without sieving (R), sieving sand (S), and wet conditions (W).

The crushing force is an important parameter to determine the binder effectiveness, either organic or inorganic binder. According to Kawatra & Ripke[69], the criteria for choosing an adequate binder should meet at least 22.5 N per pellet under the dry state. In this work the crushing force values were considerably higher than the minimum value based on the principle for an acceptable quality of a blinder so, the 3 conditions are suitable even for wet scenarios as post-combustion (Table 5). In addition to this requirement, an appropriate binder must meet other criteria such as a good resistance during drying and adequate nucleation during the palletization. The pellets resistance during drying and heating must accomplish a good resistance due to the water evaporation leads to a pressure buildup inside the pellet in which the outer layers could flake off, causing a thermal spalling[70]. In this case, the pellets dried at 450 °C showed a good drying and heating resistance owing to no pellets had any failure. This is also related to the thermal ramp used, which does not allow a sudden change in temperature to avoid the pellet breakage. On the other hand, the pelletizing process normally is carried out into pelletizing disc or pelletizing drum, in which the function of the binder is to agglomerate the particle grains, as a results a "green pellet" is formed. However in this work, the pellet elaboration method was different, therefore the quality of the natural clay as a binder in the palletization process cannot be analyzed. The most useful binder is bentonite due to the its features such as the water absorb ability, the mechanical resistance and the reasonable price[70]. The used binder in this work was natural clay without any refining treatment, which gives an extra economic value.

UNIVERSIDAD
YACHAY
TECH

SCHOOL OF
CHEMICAL SCIENCES
AND ENGINEERING

Table 5: Summary of mechanical properties of different samples under the uniaxial compression test.

Samples	Compressive strength (MPa) ± 0.66	Elastic modulus (MPa) ± 53.51	Compressive toughness (MPa) ± 0.0172	Crushing force (N) ± 76.53
C304 Dry	5.01	283.04	0.0861	625.76
C304 Wet	3.82	166.20	0.0846	457.36
C304-104 R 15%	5.60	205.56	0.1344	683.21
C304-104 R 25%	3.18	168.42	0.0771	395.00
C304-104 S 15%	6.08	292.56	0.1335	743.67
C304-104 S 25%	5.02	299.53	0.0894	616.25
C304-104 W 15%	2.70	139.72	0.0670	331.89
C304-104 W 25%	2.05	89.04	0.0515	238.21

Table 5 summarizes the mechanical properties of the control samples and clay/sand pellets at 15 and 25 wt.% for the 3 conditions: samples mixed with sieved sand, sand that was not sieved, and wet conditions. The high standard deviation values could be related to the handmade elaboration method used to elaborate the specimens; therefore, the compaction pressure was not uniform causing higher fluctuations in the mechanical properties results. The standard deviations values were averaged in Table 5, in contrast to figures which show the individual standard deviation values.

The elastic module showed the highest value for samples C304-104 S 25%, and it exceeded the results of C304-104 15 % and C304 samples with a minimum difference (Figure 12a and 12b). The standard deviation in these samples are very notable mainly caused by the elaboration method, however the results are according to the literature. Several authors proved that the porosity is inversely related to the elastic module for porous brittle materials; in fact, they reported that a higher porosity, the lower the elastic module values[71–73]. Samples mixed with sand that was sieved exhibited lower values than samples mixed with sieved sand. The wetting samples decreases the elastic modulus considerably. It is important to point out that the results of the averaged elastic modulus were achieved from the best linear fit, such that the values were greater than 0.9855.

In general, the elastic module demonstrated relatively lower values than other materials such as stainless steel (189.60 GPa), nickel alloys (206.80 GPa), and cupper (120 GPa)[74]. Although ceramics are considered brittle materials, they exhibit slight higher values than metals; for instance, aluminum oxide, silicon carbide and nitride ceramic show the higher elastic module values of about of 393 GPa, 345 GPa and 304 GPa respectively. The higher values are related to the higher temperatures (in a range of 900 and 1400 °C) that these

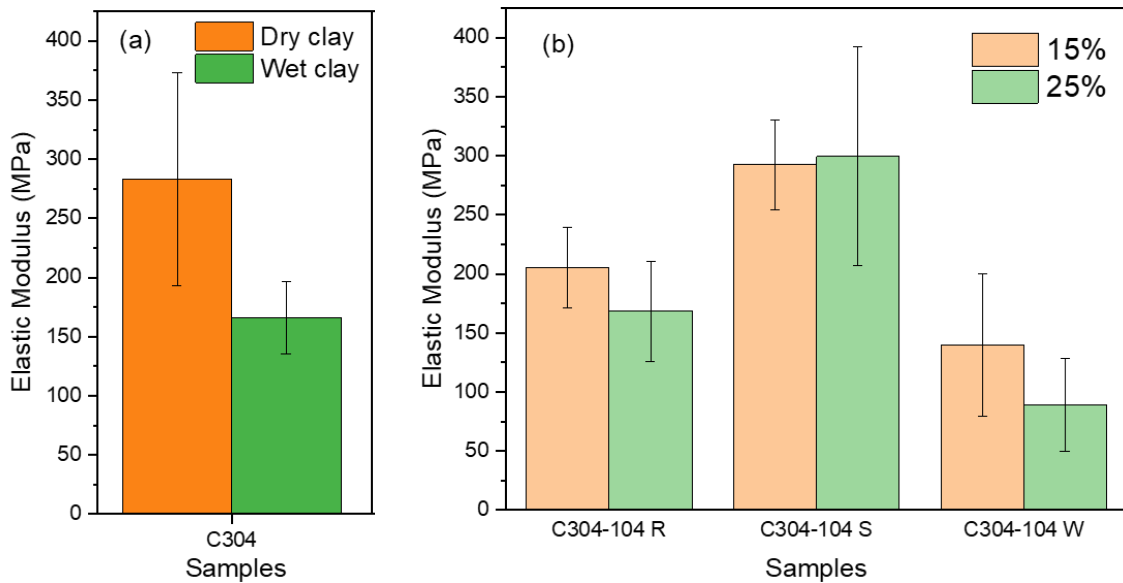materials are subjected, therefore the pore volume is reduced causing an improvement in the mechanical properties[48].

Figure 12: Elastic modulus for specimens: (a) dry and wet control samples specimens, (b) specimens with 15 and 25 wt. % of sand content at the 3 different conditions: sand without sieving (R), sieving sand (S), and wet conditions (W).

Regarding toughness, the control samples showed similar values under dry and wet conditions (Figure 13a); nonetheless, the standard deviation was higher for wet conditions. Moreover, the toughness showed similar values for C304-104 S 15% and C304-104 R 15%, however for samples with 25 wt.% sand content, the toughness decreased (Figure 13b). On the other hand, samples with 15 wt.% sand content have higher toughness values than the control samples due to they have lower porosity, therefore they have more superficial area which allow to accumulate more energy before their rupture[75]. The high compressive forces produce the energy required to crack the material; consequently, this energy disperses through the samples and leads to the surface cracks formation. Thus, the crack propagation causing the sample rupture due to the pore. The pores are considered void spaces that reduce the surface area of the material, therefore lead to a lower compression strength and lesser breakage strength. In general, the toughness values were low, which could be attributed to the brittle behavior.
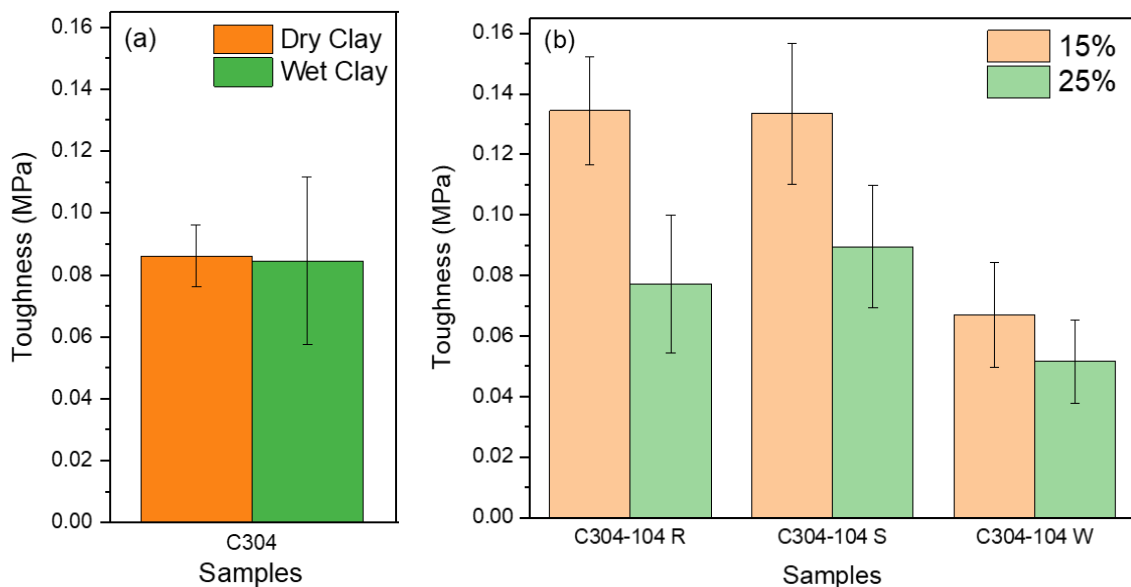
Figure 13: Toughness for specimens: (a) dry and wet control samples specimens, (b) specimens with sand content at the 3 different conditions: sand without sieving, sieving sand and wet conditions.

In general, the wet samples demonstrated the lower mechanical resistance over all conditions against uniaxial compression test. It is argued by Erguler & Ulusay[76], who demonstrated that the higher the water content in clays is, the more notable the decrease in mechanical properties. The reduction in mechanical properties may related to the development of hydraulic pressure in the pores filled with water, thus affecting the stress among grains during compression. Additionally, the minerals alteration that comprising the pellets under wet conditions can affect the mechanical properties. In this case, the samples were kept in distilled water for 6 days for analysis under extreme conditions. In this way, they were saturated with water, the reason why the noteworthy decrease in their mechanical properties under compression forces. The study of samples under wet conditions is important because during CO_2 adsorption processes at the industrial-scale, water can be present in the system. The water is either contained in the gas stream (steam water or condensed water) or it is a reaction product between CO_2 and iron oxides; hence the mechanical properties of the adsorbent could be affected.

Concerning samples mixed with sand that was not sieved demonstrated lower mechanical resistance than samples mixed with sieved sand. These results could be attributed to the higher size and quartz content in the samples. According to Sousa[77], at higher quartz contents, the compressive strength decreases due to an increase in quartz-quartz, which reduces to accommodate the deformation. A similar behavior could be attributed to the ferruginous sand because the magnetite and ilmenite have higher hardness values (around

6 in Mohs scale)[78]. Consequently, at higher sand contents, the contact among the metallic oxides and other minerals increases, thus it can lead to an easier fracture. Minerals that contain hydroxyl and water molecules (kaolinite and muscovite) have lower hardness, meaning that they are easier to break when they come into contact with other minerals with higher hardness under compressive forces.

The samples were analyzed after the fracture during the uniaxial compression test (Figure 14). It was notable that appeared longitudinal lines, which mean a brittle fracture because the crack perpendicular motion direction of the applied compressive stress[48]. The sand addition do not affect the brittle behavior of pellets, due to the same longitudinal fracture showed up (Figure 14b). Omrani et al.[79], reported in their work similar behavior for their clay and sand samples without fibers. In contrast, the addition of a plant fiber led the material to a ductile behavior.
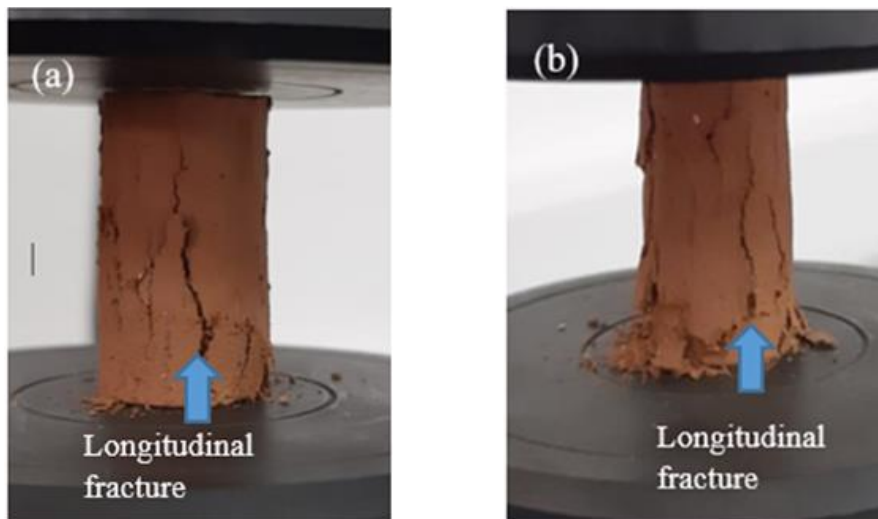

Figure 14: Specimen shapes after failure under uniaxial compression test: (a) control sample, (b) sample C304-104 S 25%.

6.2 Sample characterization of the powder by X-ray diffraction (XRD)

The diffractograms patterns for the different samples analyzed by XRD showed in Figure 15. The XRD patterns exhibited the mineral phases of the control sample, C304-104 S 15%, C304-104 S 25%, N.M. ferruginous sand, E.M. ferruginous sand and sieved ferruginous sand.
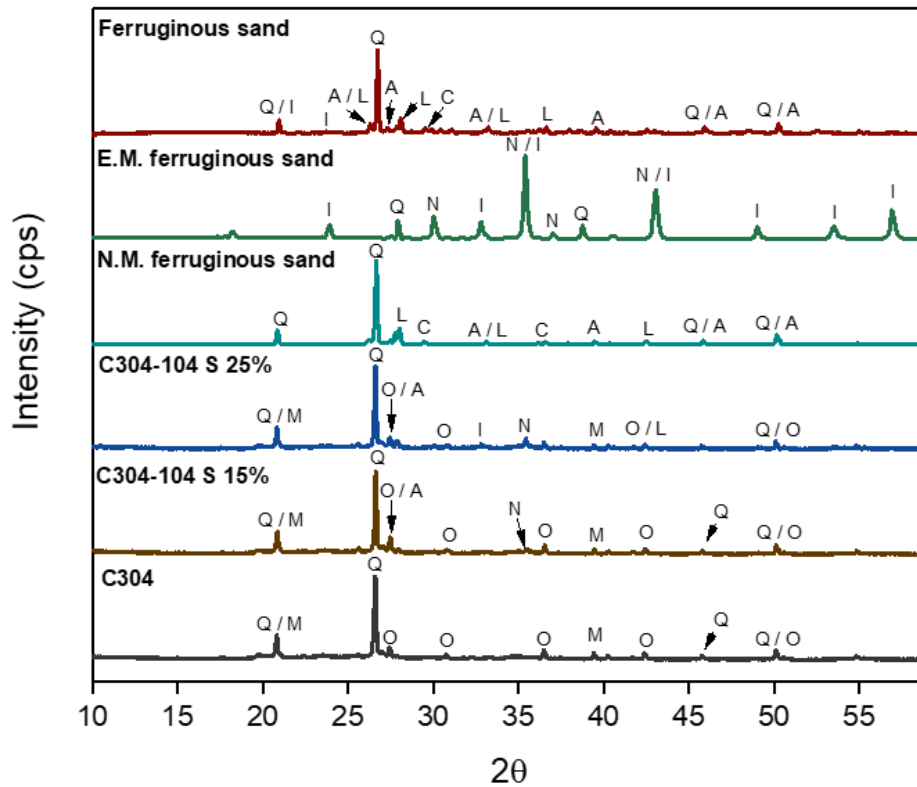
Figure 15: Diffractograms patterns of C304, C304-104 S 15%, C304-104 S 25%, N.M. ferruginous sand, E.M. ferruginous sand, and ferruginous sand. The nomenclature for the mineral phases is as follows: quartz (Q), orthoclase/microcline (O), muscovite (M), aragonite (A), magnetite (N), ilmenite (I), labradorite (L), and calcite (C).

Microcline and orthoclase were unified in a unique phase because their phases are similar. It can be observed that the strongest diffraction peak for all samples (except for E.M. ferruginous sand) came from quartz. The control sample exhibited minerals such as orthoclase/microcline (O), muscovite (M), and quartz (Q). The same mineral phases remained in the sample C304-104 S 15%, which also had at a slight peak for magnetite (N) and a stronger peak for aragonite (A). For C304-104 S 25% magnetite (N) peak was stronger, and a slight peak appeared for ilmenite (I) and labradorite (L). Regarding N.M. ferruginous sand, quartz remained as the dominant phase. It can be observed small peaks for calcite (C), and aragonite (A). Another peak attributed to labradorite (L) showed a stronger intensity than the other phases. There was not evidenced the presence of muscovite (M) from the peak at approximately 20 2θ, which confirmed that phase came from clay. In contrast, E.M. ferruginous sand showed the highest peak for magnetite and ilmenite (N, I) and medium-sized peaks for quartz (Q), therefore it indicated the magnetic phases were magnetite and ilmenite (N, I). The ferruginous sand showed the combination of the N.M. ferruginous sand and E.M. ferruginous sand, this was evidenced since the peaks agree with the same positions. The components which exhibited a percentage lower than 5% were not labeled in Figure 15.

The quantitative and qualitative analysis results are shown in table 6, the data provided there, confirmed the peaks presence in the XRD diffraction patterns (Figure 15). A large variety of mineral phases were observed due to the non-purification treatment of clay. The same peaks which appeared in the XRD patterns agree with the orthoclase/microcline, muscovite, and quartz values; so, it confirms that these mineral phases mainly make up the clay. It was also identified less content mineral phases such as albite, kaolinite, guidottiite, hematite and brookite. The addition of 15 wt.% ferruginous sand, lead to the identification of magnetite, ilmenite, calcite, aragonite, labradorite and anorthite in a minor content. Regarding C-304 S 25%, metallic oxides increased in a low percentage, however the orthoclase/microcline, muscovite, kaolinite and albite content decreases since their minerals come from clay. In contrast, quartz content remained almost constant for all the samples, except for M.E. ferruginous sand. Concerning the N.M. ferruginous sand, the non-magnetic mineral phases as shown Fig. 15 were quartz, aragonite, labradorite and calcite. Among them, calcite showed less quantity and quartz the higher. On the other hand, the E.M. ferruginous sand showed iron and ilmenite oxides, the ilmenite content represented more than half of the amount of the magnetic separation sample. Finally, ferruginous sand showed that quartz, aragonite and labradorite are the predominant phases. The metallic oxides content were relatively low, compared to the other mineral phases.

Table 6: Qualitative and quantitative analysis results of C304, C304-104 S 15%, C304-104 S 25%, ferruginous sand, N.M. Ferruginous sand and E.M. Ferruginous sand.

N°	Compound Name	COD Card	Relative abundance (%)					
			Clay C304	C304-104 S 15%	C304-104 S 25%	N.M. Ferruginous sand	E.M. Ferruginous sand	Ferruginous sand
1	Quartz	00-900-9666	44.70	37.40	37.20	48.60	13.60	38.50
2	Orthoclase/ microcline	00-101-1205	23.90	22.30	18.40	-	-	-
3	Muscovite	00-100-0042	20.40	10.70	5.10	-	-	-
4	Albite	00-900-0702	4.50	4.40	3.70	-	-	-
5	Kaolinite	00-900-9230	3.00	4.00	2.90	-	-	-
6	Guidottiite	00-901-4441	2.30	1.20	0.90	-	-	-
7	Hematite	00-210-8028	0.90	0.20	0.14	-	-	-
8	Brookite	00-900-4137	0.30	-	-	-	-	-
9	Magnetite	00-101-1496	-	0.25	0.31	-	27.70	1.80
10	Ilmenite	00-901-0915	-	3.20	4.15	-	58.70	5.30
11	Calcite	00-101-0962	-	0.84	1.20	3.60	-	7.40
12	Aragonite	02-103-1192	-	6.10	12.00	15.90	-	23.00
13	Labradorite	00-900-0744	-	7.70	11.80	31.90	-	20.30
14	Anorthite	00-900-1260	-	1.71	2.20	-	-	3.70
	(-): not present							

7. CONCLUSION AND RECOMMENDATIONS

7.1 Conclusions

This work analyzed some mechanical properties of an innovative adsorbent prepared from Ecuadorian raw materials in pellet form for CO_2 capture. The values exhibited from the free-fall drop impact and uniaxial compression tests suggested that the porosity, sand content and humidity affected the mechanical properties of this material. The results had a remarkable data dispersion associated by the handmade elaboration method.

The free-fall drop impact test demonstrated that the sand content decreased the drop number of the samples for wet and dry conditions. The dry samples showed a sharp drop between samples C304-104 1% and C304-104 5%, which indicates that the sand addition is not proportional to the drop number, it means that the samples do not behave a linear approach. Besides, the samples C304-104 S 5% and C304-104 S 50% had drop number values lower than the minimum requirement, so that pellets composition are not suitable for scaling-up. Regarding wet conditions, the drop number was the same compared to the dry samples, except for pellets with 15 wt.% sand content which demonstrated a slight increase. Thus, it can be concluded that water content in pellets do not affect the drop number, but the increase of sand content do it. Also, it was observed that the type of pellets breakage was surface fracture and a body breakage.

The mechanical properties estimated by the uniaxial compression test presented different tendencies for compressive strength, elastic module and toughness based on the porosity, the mineral composition and wet conditions. The higher values for compressive strength were attributed to samples with lesser porosity and mixed with sieved sand, in fact the sample C304-104 S 15% shower the highest compressive strength. A similar behavior was observed for elastic module; however, the sample C304-104 S 25% exhibited the highest elastic module with a minimum difference compared to C304-104 S 15%. Concerning toughness, the values were low and the results did not vary significantly, this is due to these materials are consider brittle. For all the samples the wet condition exhibited the lower mechanical resistance, however they meet the minimum requirement for their use based on the crushing force criteria. Longitudinal cracks appeared on the specimens' surface, which indicated the brittle rupture.

The XRD and the qualitative analysis revealed that as the ferruginous sand increased, oxides minerals augment. This data confirms that the ferruginous sand contains high iron and titanium oxides. In fact, the E.M. Ferruginous sand demonstrated that ilmenite predominates over magnetite.

5.2 Recommendations

Based on the experimental experience and the results, it is suggested that for further investigations take into account the following recommendations:

- To mix the sand and clay with movements from the bottom to up instead of stirrings movements.
- To elaborate the specimens using a hydraulic pressure with the respective mold in order to compact uniformly the samples and avoid the data dispersion results.
- To perform the free-fall drop impact test on surfaces more similar to the industry such as steel and also over a plate made of the same material as the binder.
- To execute the uniaxial compressive test with the samples of 1, 5, 10, 20 and 50 wt.% in order to have a broader perspective of the sand content into the samples behavior.

8. References

1. Jackson RB, Friedlingstein P, Andrew RM, Canadell JG, Quéré C Le, Peters GP. Persistent fossil fuel growth threatens the Paris Agreement and planetary health 2019;

2. National oceanic and atmospheric administration. 2013. Available from: http://www.esrl.noaa.gov/gmd/ccgg/trends

3. IPCC. Special report on emissions scenarios: a special report of working group III of the Intergovernmental Panel on Climate Change. New York: Cambridge University Press.

4. United Nations. Paris Agreement. 2015. Available from: ec.europa.eu/clima/policies/ international/negotiations/paris_en

5. Weinhofer G, Hoffmann VH. Mitigating climate change - How do corporate strategies differ? Bus Strateg Environ. 2010;19(2):77–89.

6. Yang H, Xu Z, Fan M, Gupta R, Slimane RB, Bland AE, et al. Progress in carbon dioxide separation and capture : A review. 2008;20:14–27.

7. Kelektsoglou K. Carbon Capture and Storage : A Review of Mineral Storage of CO_2 in Greece. 2018;

8. Blomen E, Hendriks C, Neele F. Capture technologies : Improvements and Promising Developments. Energy Procedia [Internet]. 2009;1(1):1505–12. Available from: http://dx.doi.org/10.1016/j.egypro.2009.01.197

9. Sifat NS, Haseli Y. A Critical Review of CO_2 Capture Technologies and Prospects for Clean Power Generation. 2019;

10. Qiao Z, Wang Z, Zhang C, Yuan S, Zhu Y, Wang J. PVAm–PIP/PS composite membrane with high performance for CO_2/N_2 separation. AIChE J. 2012;59(4):215–28.

11. Casas N, Schell J, Blom R, Mazzotti M. MOF and UiO-67/MCM-41 adsorbents for pre-combustion CO_2 capture by PSA: Breakthrough experiments and process design. Sep Purif Technol [Internet]. 2013;112:34–48. Available from: http://dx.doi.org/10.1016/j.seppur.2013.03.042

12. Suleman M, Haq I, Jamal SA. chemical absorption and hybrid system : current status and challenges. 2018;34:1–34.

13. Langlois P, Pentchev I, Hinkov I, Lamari FD, Langlois P, Dicko M, et al. CARBON DIOXIDE CAPTURE BY ADSORPTION. 2016;609–26.

14. Song C, Liu Q, Deng S, Li H, Kitamura Y. Cryogenic-based CO_2 capture

technologies: State-of-the-art developments and current challenges. Renew Sustain Energy Rev. 2019;101(July 2018):265–78. Available from: https://doi.org/10.1016/j.rser.2018.11.018

15. Han Y, Ho WSW. Recent advances in polymeric membranes for CO_2 capture. Chinese J Chem Eng. 2018;2238–54. Available from: https://doi.org/10.1016/j.cjche.2018.07.010

16. Ricaurte M, Dicharry C, Broseta D, Renaud X, Torre J. CO_2 Removal from a CO_2 − CH_4 Gas Mixture by Clathrate Hydrate Formation Using THF and SDS as Water-Soluble Hydrate Promoters. 2013;

17. Mondal MK, Balsora HK, Varshney P. Progress and trends in CO_2 capture / separation technologies : A review. Energy. 2012;46(1):431–41. Available from: http://dx.doi.org/10.1016/j.energy.2012.08.006

18. Rashidi NA, Yusup S. An overview of activated carbons utilization for the post-combustion carbon dioxide capture. Biochem Pharmacol. 2016;13:1–16. Available from: http://dx.doi.org/10.1016/j.jcou.2015.11.002

19. Arencibia A, Pizarro P, Sanz R, Serrano DP. Microporous and Mesoporous Materials CO_2 adsorption on amine-functionalized clays. Microporous Mesoporous Mater. 2019;282(March):38–47. Available from: https://doi.org/10.1016/j.micromeso.2019.03.012

20. Li JR, Kuppler RJ, Zhou HC. Selective gas adsorption and separation in metal-organic frameworks. Chem Soc Rev. 2009;38(5):1477–504.

21. Ralph Yang. Adsorbents: Fundamental and applications. Sons JW& sons, editor. New Jersey; 2003.

22. Zhang Z, Xu M, Wang H, Li Z. Enhancement of CO_2 adsorption on high surface area activated carbon modified by N_2 , H_2 and ammonia. Chemestry Engineering Journal. 2010;160(2):571–7. Available from: http://dx.doi.org/10.1016/j.cej.2010.03.070

23. Walton KS, Abney MB, Levan MD. CO_2 adsorption in Y and X zeolites modified by alkali metal cation exchange. 2006;91:78–84.

24. Zhao H, Hu J, Wang J. CO_2 Capture by the Amine-modified Mesoporous Materials. 2007;23(6):801–6.

25. Su F, Lu C, Kuo S, Zeng W. Adsorption of CO_2 on Amine-Functionalized Y-Type Zeolites. 2010;24(13):6567–74.

26. Sumida K, Rogow DL, Mason JA, Mcdonald TM, Bloch ED, Herm ZR, et al.

Carbon Dioxide Capture in Metal À Organic Frameworks. 2012;724–81.

27. Lip W, Shiun J, Hashim H, Azri A, Shin W. Review of pre-combustion capture and ionic liquid in carbon capture and storage. Appl Energy. 2016;183:1633–63. Available from: http://dx.doi.org/10.1016/j.apenergy.2016.09.103

28. Samanta A, Zhao A, Shimizu GKH, Sarkar P, Gupta R. Post-Combustion CO_2 Capture Using Solid Sorbents : A Review. 2012;1438–63.

29. Zhao Y, Cao Y, Zhong Q. CO_2 Capture on Metal-Organic Framework and Graphene Oxide Composite Using a High-Pressure Static Adsorption Apparatus. 2014;2(1):0–3.

30. Sun H, Wu C, Shen B, Zhang X, Zhang Y, Huang J. Materials Today Sustainability Progress in the development and application of CaO-based adsorbents for CO_2 capture d a review. 2018;2.

31. Alonso A, Moral-vico J, Abo A, Busquets-fité M, Komilis D, Puntes V, et al. Science of the Total Environment Critical review of existing nanomaterial adsorbents to capture carbon dioxide and methane. Sci Total Environ. 2017;595:51–62. Available from: http://dx.doi.org/10.1016/j.scitotenv.2017.03.229

32. Plaza MG, García S, Rubiera F, Pis JJ, Pevida C. Post-combustion CO_2 capture with a commercial activated carbon : Comparison of different regeneration strategies. Chemical Engineering Journal. 2010;163(1–2):41–7. Available from: http://dx.doi.org/10.1016/j.cej.2010.07.030

33. Xu C, Hedin N. Microporous adsorbents for CO_2 capture – a case for microporous polymers ? Biochem Pharmacol [Internet]. 2014;17(8):397–403. Available from: http://dx.doi.org/10.1016/j.mattod.2014.05.007

34. Zhou D, Zhang X, Mo Z, Xu Y, Tian X, Li Y, et al. Adsorptive separation of carbon dioxide: from conventional porous materials to metal–organic frameworks. EnergyChem. 2019;100016. Available from: https://doi.org/10.1016/j.enchem.2019.100016

35. Badaniˇ M, Zele V, Halamová D, Cejka J, Zukal A, Murafa N, et al. Amine-modified ordered mesoporous silica : Effect of pore size on carbon dioxide capture. 2008;144:336–42.

36. Da E. Microporous and Mesoporous Materials Adsorption of heavy metals on functionalized-mesoporous silica : A review. Microporous Mesoporous Mater. 2017;247:145–57. Available from:

http://dx.doi.org/10.1016/j.micromeso.2017.03.050

37.   Ma Y, Wang Z, Xu X, Wang J. Review on porous nanomaterials for adsorption and photocatalytic conversion of CO_2. Chinese J Catal. 2017;38(12):1956–69. Available from: http://dx.doi.org/10.1016/S1872-2067(17)62955-3

38.   Pham T, Lee B, Kim J, Lee C. Enhancement of CO_2 capture by using synthesized nano-zeolite. J Taiwan Inst Chem Eng [Internet]. 2016;0:1–7. Available from: http://dx.doi.org/10.1016/j.jtice.2016.04.026

39.   Zhang J, Webley PA, Xiao P. Effect of process parameters on power requirements of vacuum swing adsorption technology for CO_2 capture from flue gas. 2008;49:346–56.

40.   Basnayake SA, Su J, Zou X, Balkus KJ. Carbonate-Based Zeolitic Imidazolate Framework for Highly Selective CO_2 Capture. 2014;

41.   Chouikhi N, Cecilia JA, Vilarrasa-garc E, Besghaier S, Chlendi M, Ignacio F, et al. CO_2 Adsorption of Materials Synthesized from Clay Minerals : A Review. 2019;1–22.

42.   Chen Y, Lu D. Applied Clay Science CO_2 capture by kaolinite and its adsorption mechanism. Applied Clay Science. 2015;104:221–8. Available from: http://dx.doi.org/10.1016/j.clay.2014.11.036

43.   Hakim, A., Marliza, T. S., Tahari N. M., WanW. N. Yusop N. R., Mohamad, M. W., and Yarmo AM. Studies on CO_2 Adsorption and Desorption Properties from Various Type Iron Oxides (FeO ,. 2016;

44.   Gorospe A. Proyectos de Mineria en Ecuador. Quito; 2018.

45.   Uribe R. Investigaciones de Materias Primas Minerales No Metálicas en el Ecuador. 2015;36(3):34–44.

46.   Ani T Al. Clay and clay mineralogy. 2018;(September).

47.   Chuquirima M. Estudio y obtencion de metal de hierro a partir de areas ferruginosas. Escuela Politenica Nacional, Quito- Ecuador; 2014.

48.   Callister W, Rethwisch D. Materials Science and Engineering an Introduction. Wiley, editor. Ney Jersey; 2010.

49.   Tick Links. Stress Strain Graph & Classification of Material [Internet]. 2016. Available from: https:%0A//www.youtube.com/watch?v=xQHz3MsHHwo

50.   Miller DC, Litynski JT, Brickett LA, Morreale BD. Capture Systems. 2016;62(1).

51.   Luna S. Clay - iron oxide biphasic agglomerate as sorbent applied to hydrogen sulfide capture. Yachay tech, Urcuqui-Ecuador.; 2019.

52. Vera D. Characterization of Ecuadorian Ferruginous and Titaniferous Sands for Hydrogen Sulfide Capture. Yachay Tech University, Urcuqui-Ecuador.; 2020.

53. Jimenez M. Characterization of pellets from raw clays for their potential adsorption of H_2S in gas sweeting streams. Yachay Tech University, Urcuqui-Ecuador.; 2020.

54. Axelsson L, Franzén M, Ostwald M, Berndes G, Lakshmi G, Ravindranath NH. Perspective: Jatropha cultivation in southern India: Assessing farmers' experiences. Biofuels, Bioprod Biorefining. 2012;6(3):246–56.

55. Altomare A, Correiro N, Coucci C, Falcicchio A, Moltineri A, Rizzi R. A qualitative phase analysis software using the freely available database POW_COD. J Appl Crystallogr. 2015;

56. Grazulis S, Chateigner D, Downs R, Yokochi A, Quiros M, Lutterotti L, et al. Crystallography Open Database-an open-access collection of crystal structures. J Appl Crystallogr [Internet]. 2009; Available from: https://doi.org/10.1107/S0021889809016690

57. Hanawalt JD. Manual Search/Match Methods for Powder Diffraction in 1986. Powder Diffraction. 1986; Available from: https://doi.org/10.1017/S0885715600011209

58. Toraya H. Whole-Powder-Pattern Fitting Without Reference to a Structural Model: Application to X-ray Powder Diffractometer Data. J Appl Crystallogr [Internet]. 1986; Available from: https://doi.org/10.1154/S0376030800015494

59. Tavares LM, de Almeida RF. Breakage of green iron ore pellets. Powder Technol. 2020;366:497–507.

60. Gul A, Sirkeci AA, Boylu F, Guldan G. IMPROVEMENT OF MECHANICAL STRENGTH OF IRON ORE PELLETS USING RAW AND. 2014;51(1):23–36.

61. Tavares LM, Cavalcanti PP, de Carvalho RM, da Silveira MW, Bianchi M, Otaviano M. Fracture probability and fragment size distribution of fired Iron ore pellets by impact. Powder Technol [Internet]. 2018;336:546–54. Available from: https://doi.org/10.1016/j.powtec.2018.06.036

62. Iljana M, Kemppainen A, Paananen T, Mattila O, Pisilä E. International Journal of Mineral Processing Effect of adding limestone on the metallurgical properties of iron ore pellets. Int J Miner Process [Internet]. 2015;141:34–43. Available from: http://dx.doi.org/10.1016/j.minpro.2015.06.004

63. Tavares LM, King RP. Modeling of particle fracture by repeated impacts using continuum damage mechanics. Powder Technol. 2002;123(2–3):138–46.

64. Cavalcanti PP, de Carvalho RM, das Chagas AS, da Silveira MW, Tavares LM. Surface breakage of fired iron ore pellets by impact. Powder Technol. 2019;342:735–43. Available from: https://doi.org/10.1016/j.powtec.2018.10.044

65. Sivrikaya O, Arol Aİ. International Journal of Mineral Processing An investigation of the relationship between compressive strength and dust generation potential of magnetite pellets. Int J Miner Process [Internet]. 2013;123:158–64. Available from: http://dx.doi.org/10.1016/j.minpro.2013.06.006

66. Austin LG. The analysis of repeated breakage events as an equivalent rate process. 1990;63:141–7.

67. Tavares LM. Analysis of particle fracture by repeated stressing as damage accumulation. Powder Technol [Internet]. 2009;190(3):327–39. Available from: http://dx.doi.org/10.1016/j.powtec.2008.08.011

68. Howarth D, Rowlands J. Development of an index to quantify rock texture for qualitative assessment of intact rock properties. Geotech Test. 1986; Available from: https://doi.org/10.1520/GTJ10627J]

69. Kawatra SK, Ripke SJ. Pelletizing steel mill desulfurization slag. 2002;65:165–75.

70. Eisele TC, Kawatra SK. Mineral Processing and Extractive Metallurgy Review A review of binders in iron ore pelletization. 2010;7508(2003).

71. Asmani M, Kermel C, Leriche A, Ourak M. Influence of porosity on Youngs modulus and poisson's ratio in alumina ceramics. J Europe Ceramic Society. 2001;21(8):1081–6.

72. Schöpfer MPJ, Abe S, Childs C, Walsh JJ. The impact of porosity and crack density on the elasticity, strength and friction of cohesive granular materials: Insights from DEM modelling. Int J Rock Mech Min Sci. 2009;46(2):250–61.

73. Nakata Y, Kato Y, Hyodo M. One-dimenssional compression behavior of uniformly graded sand related to single particle crushing strength. Soils Found Japanese Geotech Soc. 2001;

74. Davis J. Metals Handbook. Ohio: American Society for Metals; 1998.

75. Kuruppu MD, Chong KP. Fracture toughness testing of brittle materials using semi-circular bend (SCB) specimen. Eng Fract Mech. 2012;91:133–50. Available from: http://dx.doi.org/10.1016/j.engfracmech.2012.01.013

76. Erguler ZA, Ulusay R. International Journal of Rock Mechanics & Mining Sciences Water-induced variations in mechanical properties of clay-bearing rocks. 2009;46:355–70.

77. Sousa LMO. The influence of the characteristics of quartz and mineral deterioration on the strength of granitic dimensional stones. Environ Earth Sci. 2013;69(4):1333–46.

78. Hu P, Zhang S, Wang H, Pan D, Tian J, Tang Z, et al. Heat treatment effects on Fe_3O_4 nanoparticles structure and magnetic properties prepared by carbothermal reduction. J Alloys Compd. 2011;509(5):2316–9.

79. Omrani H, Hassini L, Benazzouk A, Beji H, Elcafsi A. Elaboration and characterization of clay-sand composite based on Juncus acutus fibers. Constr Build Mater. 2020;238:117712. Available from: https://doi.org/10.1016/j.conbuildmat.2019.117712

9. Annex

1. Appendix 1: Stress vs. Strains graphics
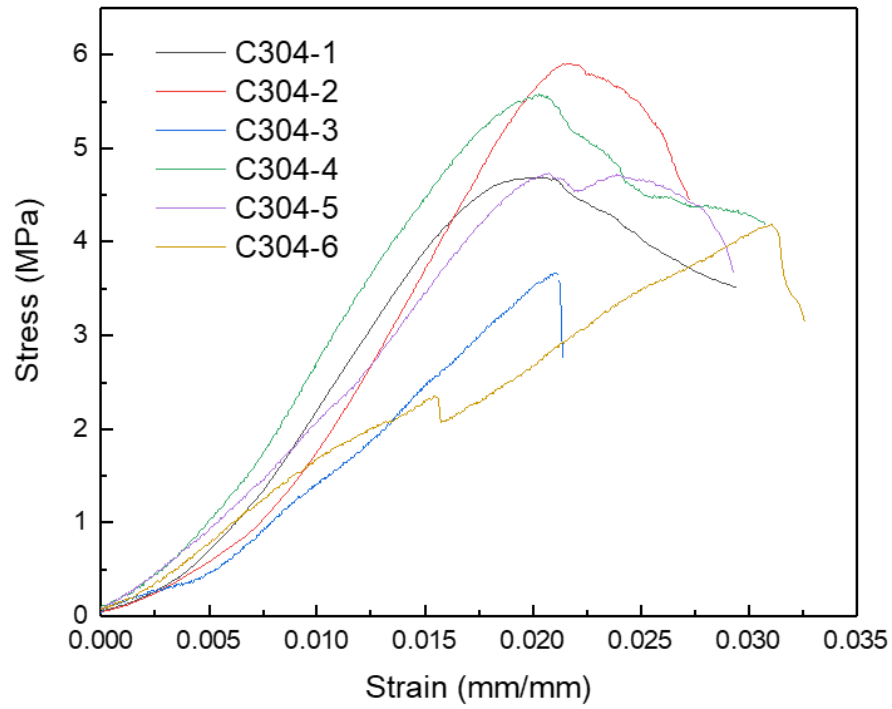
Figure 16: Stress vs. strain curve of samples C304.
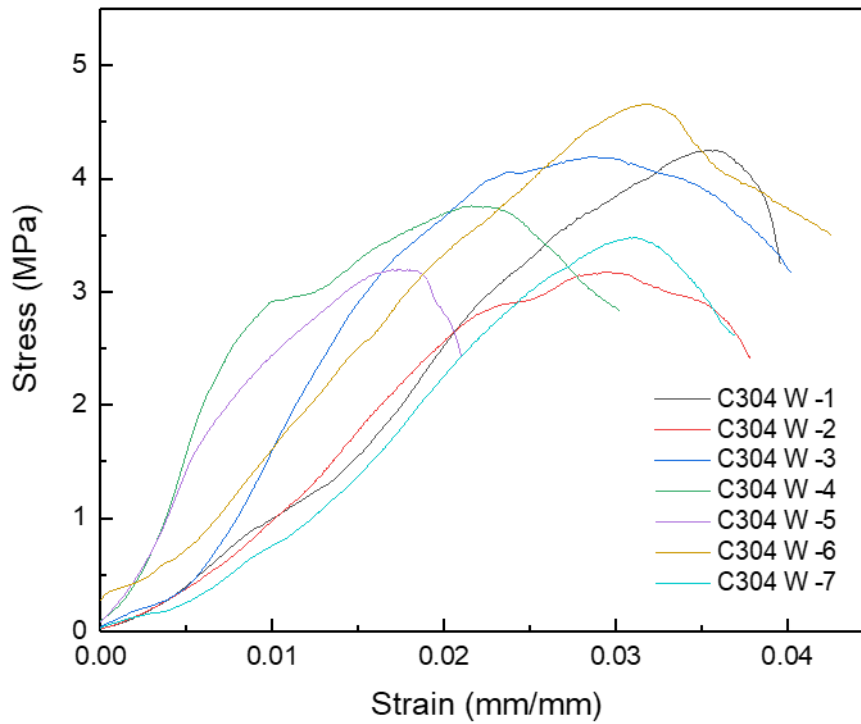
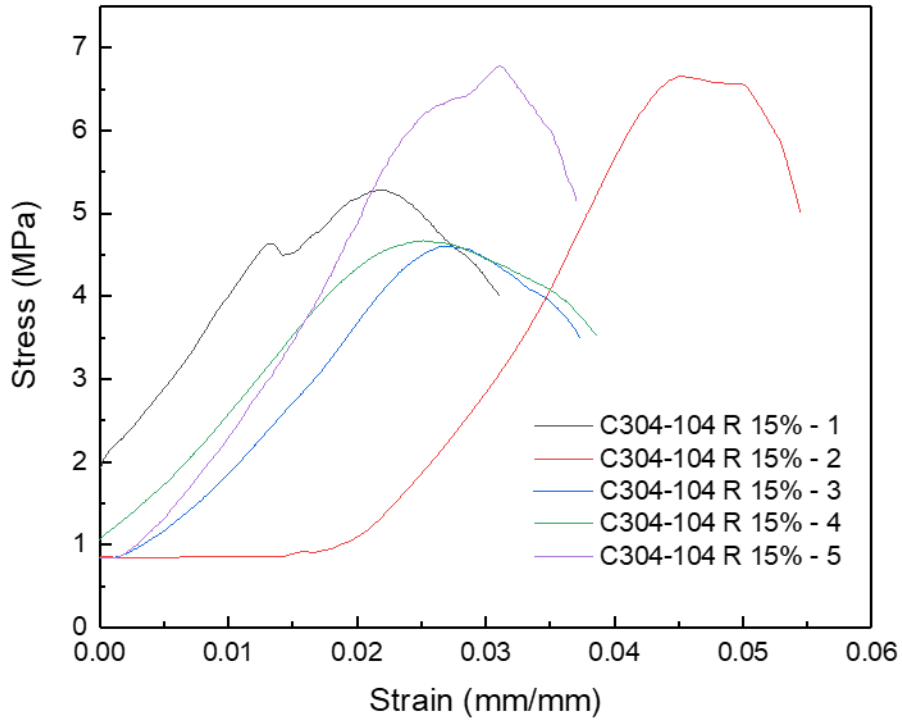**Figure 17:** Stress vs. strain curve of samples C304 W.

UNIVERSIDAD
YACHAY
TECH

SCHOOL OF
CHEMICAL SCIENCES
AND ENGINEERING

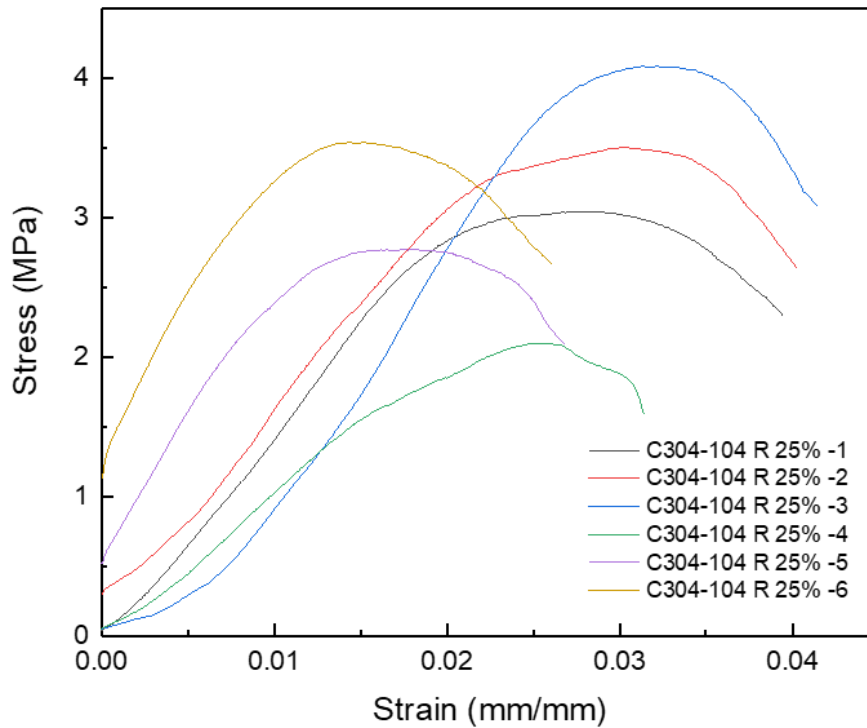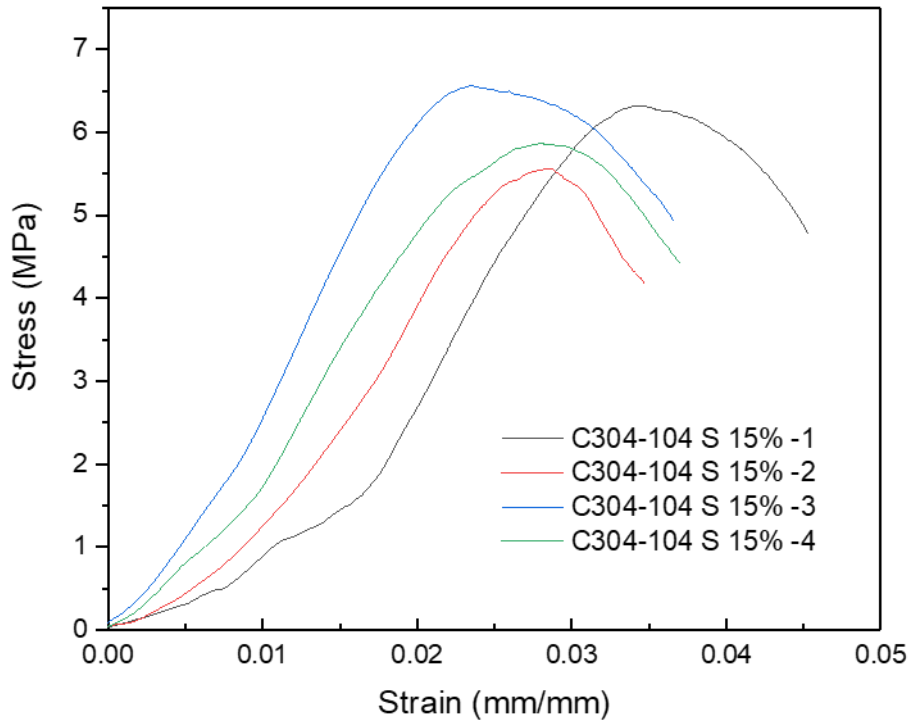**Figure 18:** Stress vs. strain of samples C304-104 R 15%

Figure 19: Stress vs. strain curve of samples C304-104 R 15%

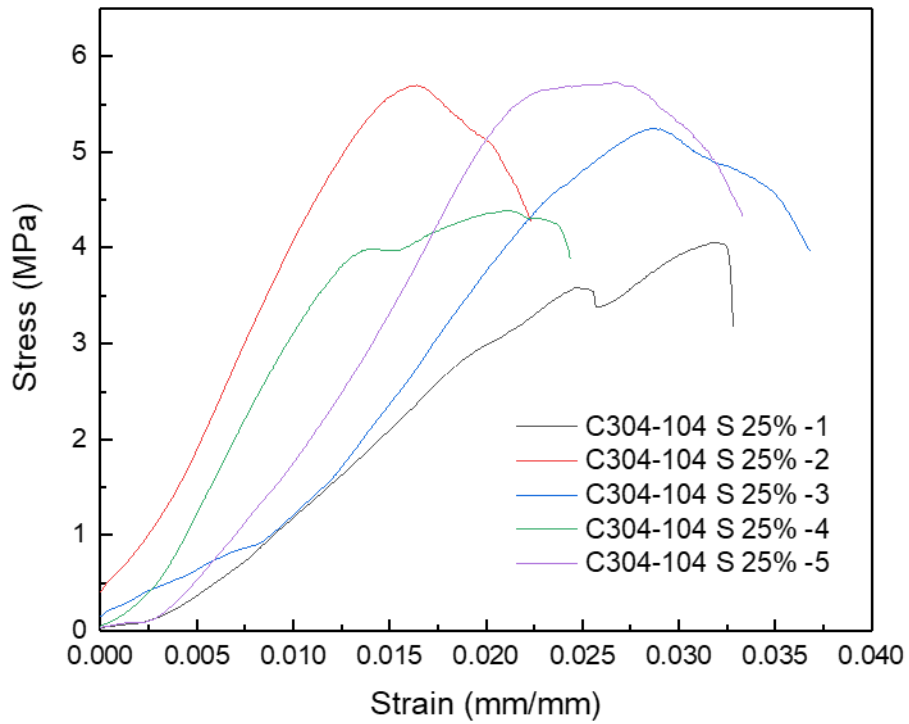**Figure 20:** Stress vs. strain curve of samples C304-104 S 15%

Figure 21: Stress vs. strain curve of samples C304-104 S 25%.

UNIVERSIDAD
YACHAY
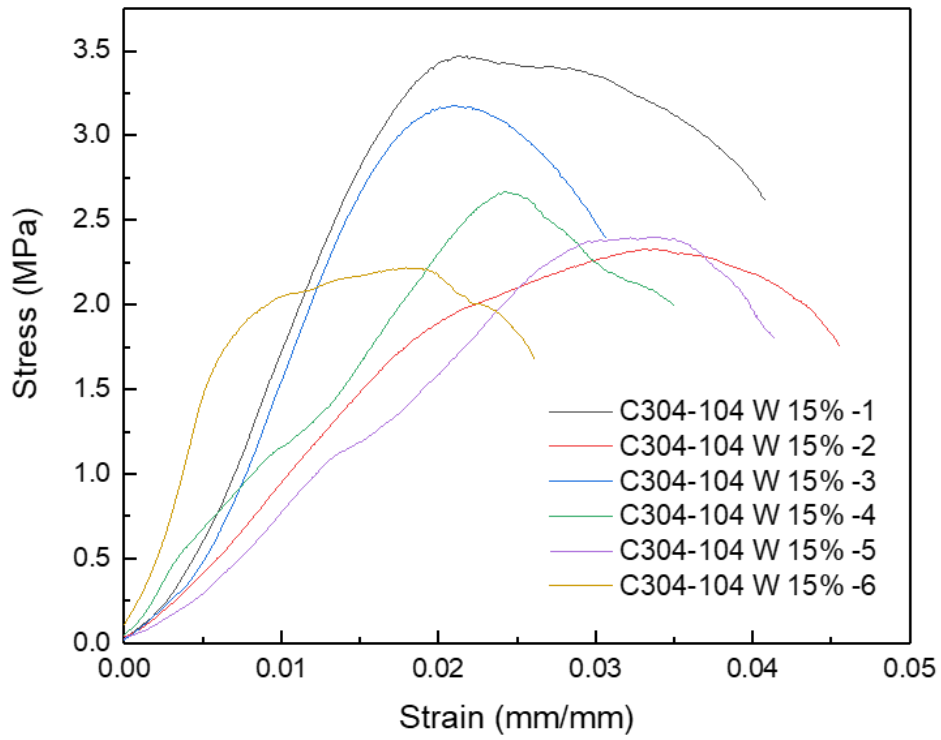TECH

SCHOOL OF
CHEMICAL SCIENCES
AND ENGINEERING
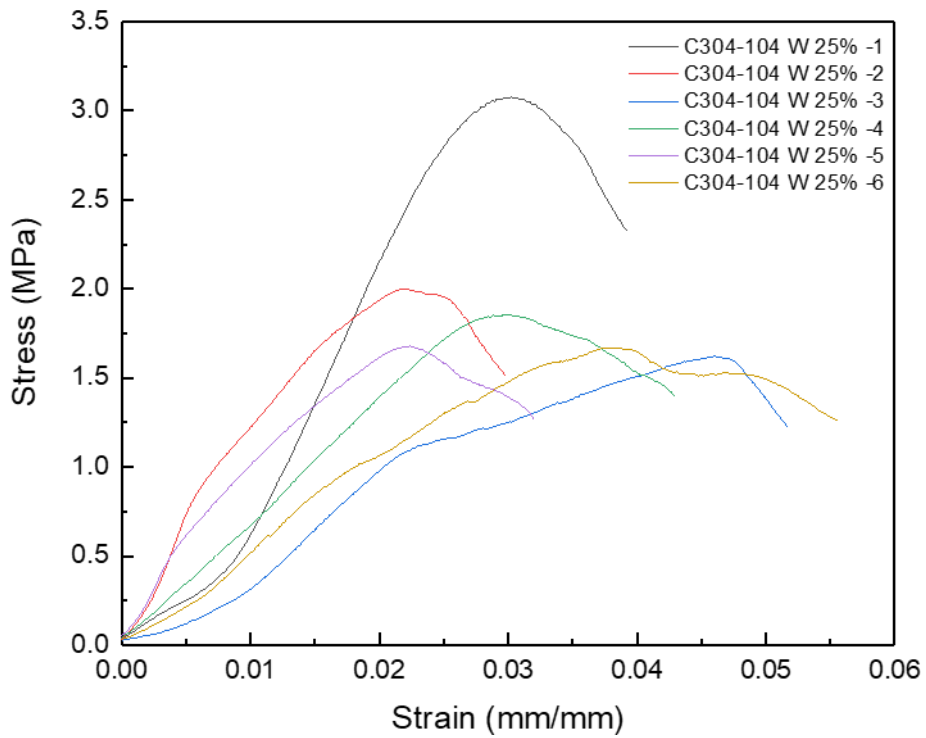
Figure 22: Stress vs. strain curve of samples C304-104 W 15%

Figure 23: Stress vs. strain curve of samples C304-104 W 25%